DISSERTATIONES
GEOLOGICAE
UNIVERSITATIS
TARTUENSIS
42

MIKK GAŠKOV

Stable isotope and fluid inclusion evidence of multistage fluidal activity in Baltic paleobasin: Silurian carbonate sequence in Kalana, Estonia

TARTU ÜLIKOOL
1632
UNIVERSITAS TARTUENSIS

DISSERTATIONES GEOLOGICAE UNIVERSITATIS TARTUENSIS
42

DISSERTATIONES GEOLOGICAE UNIVERSITATIS TARTUENSIS
42

MIKK GAŠKOV

Stable isotope and fluid inclusion evidence of multistage fluidal activity in Baltic paleobasin: Silurian carbonate sequence in Kalana, Estonia

UNIVERSITY OF TARTU
Press

Department of Geology, Institute of Ecology and Earth Sciences, Faculty of Science and Technology, University of Tartu, Estonia.

This dissertation is accepted for the commencement of the degree of Doctor of Philosophy in Geology at the University of Tartu on the 5th of June 2017 by the Scientific Council of the Institute of Ecology and Earth Sciences, University of Tartu.

Supervisors: Kalle Kirsimäe, Department of Geology, University of Tartu, Estonia

Argo Jõeleht, Department of Geology, University of Tartu, Estonia

Opponent: Krister Sundblad, Professor, Department of Geography and Geology, University of Turku, Finland

This thesis will be defended at the University of Tartu, Estonia, Chemicum, Ravila 14A, room 1019, on the 30th of August 2017 at 12:15.

Publication of this thesis is granted by the Institute of Ecology and Earth Sciences, University of Tartu and by the University of Tartu ASTRA Project PER ASPERA Doctoral School of Earth Sciences and Ecology (2014-2020.4.01.16-0027), created under the auspices of the European Regional Development Fund.

ISSN 1406-2658
ISBN 978-9949-77-524-8 (print)
ISBN 978-9949-77-525-5 (pdf)

Copyright: Mikk Gaškov, 2017

University of Tartu Press
www.tyk.ee

CONTENTS

LIST OF ORIGINAL PUBLICATIONS

This thesis is based on the following published papers, which are referred to in the text by their Roman numerals. The papers are reprinted by kind permission of the publishers.

I Eensaar, J., **Gaškov, M.,** Pani, T., Sepp, H., Somelar, P., Kirsimäe, K. 2017a. Hydrothermal fracture mineralization in the stable cratonic northern part of the Baltic Paleobasin: sphalerite fluid inclusion evidence. *GFF*, 139(1): 52–62.

II Eensaar, J., Pani, T., **Gaškov, M.**, Sepp, H., Kirsimäe, K. 2017b. Stable isotope composition of hypogenic speleothem calcite in Kalana (Estonia) as a record of microbial methanotrophy and fluid evolution. *Geological Magazine*, 154(1): 57–67.

III **Gaškov, M.**, Sepp, H., Pani, T., Paiste, P., Kirsimäe, K. 2017. Barite mineralization in Kalana speleothems, Central Estonia: Sr, S and O isotope characterization. *Estonian Journal of Earth Sciences*, 66(3): 130–141.

Author's contribution:

Paper I: The author was responsible for sample collection, analysis and interpretation of stable isotope and mineralogical data, synthesis of analytical data and in part for writing the manuscript.

Paper II: The author participated in data collection and was primarily responsible for interpretation of analytical results, synthesis of mineralogical-geochemical data and writing of the manuscript.

Paper III: The author was primarily responsible for planning research, preparation and running the analyses, data collection and synthesis, and writing of the manuscript.

1. INTRODUCTION

Geofluids play a paramount role in the evolution of the Earth. Fluids of different origin are responsible for the behavior of rock deformations, nature of volcanic eruptions, the formation of Earth resources including oil and hydrothermal mineral deposits, and most possibly have had an utmost importance in the origin and evolution of the life.

Baltoscandia that encompasses the Fennoscandian Shield and Baltic palaeobasin is one of the most stable cratonic areas of the world. This is highlighted by the apatite fission track (AFT) ages of 500 to 800 Ma in southern Finland that are the oldest documented on Earth (Hendriks et al., 2007a). Although magmatic activity in the southern Baltic palaeobasin, in Lithuania, extends to the Late Palaeozoic (Motuza et al., 2015), in the northern part of the basin there is no indication of major, large scale tectonic activity in the Phanerozoic (Puura and Vaher, 1997). As a result of the generally stable tectonic development, the Neoproterozoic-Phanerozoic sedimentary sequence in the Baltic palaeobasin has been preserved untectonized and unmetamorphosed. Organic material maturation indicators (such as reflectivities of vitrinite, chitinozas and acritarchs and biomarker ratios) suggest maximum temperatures up to 125 °C, 80–90 °C and 50–80 °C in the southwestern, central and northern parts of the basin, respectively (Lazauskienė and Marshall, 2002; Zdanavičiūtė and Swadowska, 2002; Talyzina et al., 2000), which is in agreement with the traditional interpretation of the geological evolution of the basin. The immature sedimentary organic material indicators in the northern part of the Baltic palaeobasin are, however, in conflict with the diagenetic grade of the clay minerals and palaeomagnetic remagnetization of the rocks, which suggest either much deeper burial (>2 km) or that a series of basin wide (hydrothermal) fluid intrusions/thermal perturbations occurred during the development of the basin (Hints et al., 2008; Hints et al., 2006; Kiipli et al., 2007; Kirsimäe and Jorgensen, 2000; Kirsimäe et al., 1999; Plado et al., 2010; Plado et al., 2008; Preeden et al., 2009; Preeden et al., 2008; Somelar et al., 2010; Somelar et al., 2009). Nevertheless, the low compaction of the Palaeozoic clays with porosity >20% (Kirsimäe et al., 1999) and interpretation of the AFT data do not support deep and extensive burial, at least on the eastern-southern margins of Fennoscandia (Hendriks et al., 2007a). This geological evidence suggests that the overall stable development of the Baltic palaeobasin was interrupted by a series of fluid/thermal events and possibly tectonic reactivation since around 500 Ma. Complex vertical and lateral diagenetic gradients in the basin fill (Somelar et al., 2010) suggest that the fluid migration was fracture-controlled, with the most intense alteration occurring in zones of enhanced permeability. The fault structures of the Precambrian crystalline basement may have been recurrently reactivated during tectonic stresses in the Phanerozoic and gave rise to fluid circulation systems.

As an example, occurrences of galena and sphalerite vein mineralization accompanying secondary dolomitization in the northern part of the Baltic palaeobasin have been described primarily in relation to fracture zones that intersect the Palaeozoic (Ediacaran – Devonian) sedimentary sequence in Estonia (Palmre, 1967; Pichugin et al., 1976; Puura and Vaher, 1997; Raudsep, 1997; Sundblad et al., 1999). Sulphide mineralization has also been described in the north-eastern wall of the buried Ordovician Kärdla meteorite impact crater (Suuroja, 2002) and in Ediacaran sandstones in northern Estonia (Sundblad et al., 1999). Most of these prominent occurrences of mineralizations are related to karstified southwest-northeast trending fault zones that intersect the Ordovician-Silurian carbonate sequence in central Estonia (Figure 1), and are interpreted to be of hydrothermal origin, however, neither the composition nor physical characteristics of those fluids have been studied in detail.

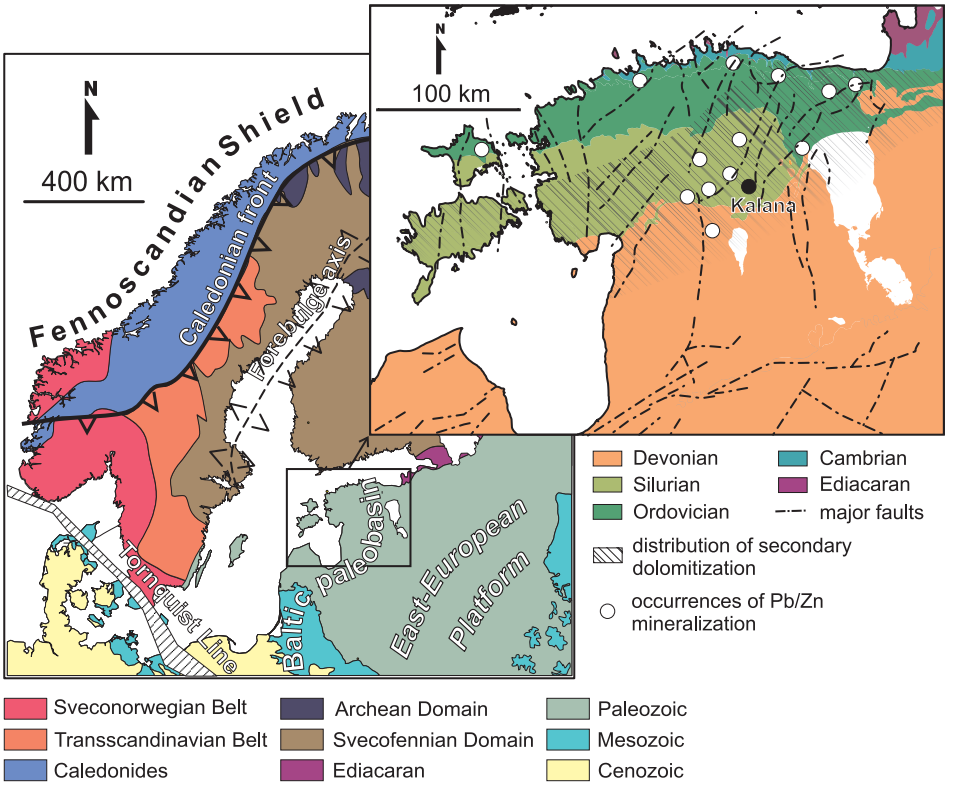

Figure 1. Schematic geological map of the study area and location of the Kalana quarry (from Eensaar et al., 2017a – PAPER I).

As an example, occurrences of galena and sphalerite vein mineralization accompanying secondary dolomitization in the northern part of the Baltic palaeobasin have been described primarily in relation to fracture zones that intersect the Palaeozoic (Ediacaran – Devonian) sedimentary sequence in Estonia (Palmre,

1967; Pichugin et al., 1976; Puura and Vaher, 1997; Raudsep, 1997; Sundblad et al., 1999). Sulphide mineralization has also been described in the north-eastern wall of the buried Ordovician Kärdla meteorite impact crater (Suuroja, 2002) and in Ediacaran sandstones in northern Estonia (Sundblad et al., 1999). Most of these prominent occurrences of mineralizations are related to karstified southwest-northeast trending fault zones that intersect the Ordovician-Silurian carbonate sequence in central Estonia (Figure 1), and are interpreted to be of hydrothermal origin, however, neither the composition nor physical characteristics of those fluids have been studied in detail.

Succession of shallowing-upward shelf carbonates of early Aeronian (Llandovery, Silurian period, c. 440 Ma) age exposed in the Kalana quarry, central Estonia, occurs next to 1–4 km wide southwest-northeast oriented linear fracture zone intersecting Palaeozoic sedimentary cover and the crystalline basement in northeast and central Estonia (Puura and Vaher, 1997). The normally bedded carbonate succession in the Kalana quarry is cut by a series of sub-parallel and vertical to sub-vertical fractures and veins that are a few to tens of centimetres wide whereas some of the veins-fracture zones are widened by karst-forming processes and constitute small cave-like structures that stretch along the fractures. Both the fractures and the cave-like structures show mineralogy mainly characterized by calcite, dolomite, barite, pyrite, sphalerite and rarely galena, possibly reflecting different phases of fluidal activity.

The aim of this thesis is to study the fluid-driven mineralization, mineral assemblage and paragenesis and fluid characteristics in fracture-controlled cave and vein systems in the Silurian carbonate succession in Kalana, central Estonia. The overall goal of this study is to constrain the origin and evolution of these mineralizing fluids in relation to Phanerozoic geodynamic processes in the Baltica continent and its margins.

2. GEOLOGICAL SETTING

The Baltic palaeobasin is a shallow, epicontinental sedimentary basin at the southern margin of the Fennoscandian Shield. Neoproterozoic-Phanerozoic deposits fill a slowly subsided epicontinental sea and the subsequent Caledonian foreland basin. The mixed siliciclastic-carbonate deposits are thickest (>2000 m) and most complete in the southwestern part of the basin, but in the northern and central parts of the basin (Estonia, northern Latvia and northwestern Russia), only Neoproterozoic Ediacaran and Lower Palaeozoic deposits occur (Nikishin et al., 1996).

The Late Neoproterozoic and Phanerozoic deformation of the basement and accumulation in the Baltic palaeobasin were governed by the passive margin development of the Iapetus Ocean and Tornquist Sea. The tectonic reconfiguration of the area was initiated by the collision of Baltica with Laurentia in the Late Silurian to Devonian (Torsvik and Rehnström, 2003), which produced the Scandinavian Caledonides orogenic suture. At the same time, the German–Polish Caledonides developed along the southern border of the plate following the closure of the Tornquist Sea (Ziegler, 1987). The amalgamation of Laurussia into Pangaea in the Carboniferous did change the tectonic configuration of the sedimentary history in the eastern Baltic palaeobasin, and except the short-term late Permian transgression (Paškevicius, 1997), the sedimentary basin temporarily retreated from the eastern Baltic region for an epoch lasting from the Carboniferous to the Permian. The younger history of the Baltic palaeobasin, which was then in the interior of amalgamated Pangaea, was mainly influenced by the breakup of the supercontinent and the opening of the Atlantic Ocean. The formation of an ephemeral marine basin in the Mesozoic, which comprised a temporary extension from the south and/or southwest into the predominantly continental study area in the Early Triassic, Middle to Late Jurassic and Albian–Maastrichtian (Paškevicius, 1997; Usaityte, 2000), was controlled by sea level changes and dynamic rifting processes in the North Sea area and in Central Europe. Marine deposition in the basin was also renewed for two short episodes in southwestern Lithuania in the Palaeocene and Pliocene.

The studied material was sampled in the Kalana quarry, central Estonia, where a succession carbonates of early Aeronian (Llandovery, Silurian period, c. 440 Ma) age is exposed (Figure 1). The quarry is located south of an area where 1–4 km wide southwest-northeast oriented linear fracture zone intersects Palaeozoic sedimentary cover and the crystalline basement in northeast and central Estonia (Puura and Vaher, 1997).

The succession is characterized by a series of shallowing-upward shelf carbonates that belong to the Raikküla Regional Stage (Männik et al., 2016; Tinn et al., 2009). As evidenced by lenses of (occasionally cross-bedded) carbonate grainstones and calcareous tempestite beds, the shelf carbonates were deposited at or close to wave-base depths in the middle–upper part of the succession.

Unusual to Estonian bedrock strata, that are homoclinal and slightly dipping (6–18') southward (Puura and Vaher, 1997), the carbonate rocks in Kalana quarry show dip up to 8–9° and are gently folded. Also, the normally bedded carbonate succession in the Kalana quarry is cut by a series of sub-parallel and vertical to sub-vertical fractures and veins that are a few to tens of centimetres wide. Most of these fractures are SW–NE oriented along the fold axial plane and occur typically in the hinge zone of folds. Some of the fracture zones are widened by karst-forming processes and constitute small caves that stretch along the fractures (Eensaar et al. 2017b – PAPER II).

The limestones exposed in the quarry are partly dolomitized. Southwest-northeast oriented fractures typically border the dolomitized zones. The palaeomagnetic remagnetization of the Silurian carbonate rocks in the Kalana quarry points to late Palaeozoic – Triassic overprinting, which is interpreted to represent low-temperature fluid activity related to the formation of the Pangea supercontinent (Preeden et al., 2008).

The cave and fracture structures are mostly found in the central and southern parts of the quarry in sub-vertical contact zones between limestone and dolomite bodies, in an about 2 m high zone at the base of the 10–15 m high quarry wall. The cave structures are typically small – up to 0.5–1 m wide, up to 15 m long and 1.5 m in height. Larger structures are filled with calcite speleothem-type deposits in association with spar calcite and euhedral barite crystal aggregates, and locally pyrite. Barite, spar calcite and pyrite mineralization are also found in the narrower fractures/veins where botryoidal calcite speleothems are absent.

3. MATERIALS AND METHODS

Calcite-sphalerite veins in the Kalana quarry were sampled in three different locations (see Figure 2 in Eensaar et al., 2017a – PAPER I). The sampled material included the calcite- and sphalerite-mineralized veins. Botryoidal calcite precipitates were collected in the southern part of the quarry (see Figure 1 in Eensaar et al., 2017b – PAPER II) where a 0.5–0.7 m wide and 1.5 m high and approximately 10 m long cave-like structure was opened in 2009. As Kalana quarry is in active operation, the cave structure is not preserved. Representative collection of different speleothems and wall rock material is deposited and available at the Natural History Museum and Department of Geology, University of Tartu (collection No. 1690). Studied barite aggregates were collected in different cave systems and fractures/veins all over the quarry including the barite associated with botryoidal speleothem crusts in the same cave-like structure where calcite precipitates were sampled. In addition to mineralized veins and speleothems, the limestone–dolomite host rocks were sampled all over the quarry.

Polished slabs and petrographic thin sections were prepared and studied using a petrographic optical microscope and a scanning electron microscope (SEM). The SEM was a variable pressure Zeiss EVO MA15 SEM equipped with an Oxford X-MAX energy dispersive detector system (EDS) and IncaWave700 wavelength dispersive (WDS) detectors, and INCA and AZTEC software for element analysis and distribution mapping. Chemical analyses were made using the EDS and WDS detectors based on a calibration with mineral standards: Ca – calcite, Mg – dolomite, Mn – rodonite, Fe – hematite, Ba – barite, Sr – celestite. For WDS analyses the counting times were 300 s at the peak and 200 s for the background. The detection limits were 100 ppm for Ca and Mg, 50 ppm for Mn and Sr, 60 ppm for Ba and 80 ppm for Fe. Additionally, X-ray fluorescence mapping of a polished slabs was performed using a Rigaku Primus II spectrometer with a 1 mm spot size.

The mineral composition of selected samples from the calcite-sphalerite veins, the calcite speleothem–like precipitates and the barite was studied by means of X-ray diffractometry. Microdrilled samples were pulverized by hand in an agate mortar, and unoriented preparations were made on a low background silicon mono-crystal sample holder or standard sample holders in cases when enough material was present. The preparations were scanned using a Bruker D8 Advance diffractometer using CuKα radiation and a LynxEye positive sensitive detector in the 2–70° 2θ range. The quantitative mineralogical compositions of the samples were interpreted and modelled using the Rietveld algorithm-based program Siroquant-3 (Taylor, 1991).

Stable isotope ratios of $\delta^{18}O$ and $\delta^{13}C$ in calcite and dolomite were measured in micro-drilled powdered samples on a Thermo Scientific Delta V Advantage continuous flow isotope ratio mass spectrometer with the precision (2σ) of 0.1‰. Reproducibility was better than ±0.1‰ for $\delta^{18}O$ and ±0.1‰ for $\delta^{13}C$. The

results of carbonate mineral analyses are expressed in per mil deviation relative to the Vienna PeeDee Belemnite (VPDB) scale for oxygen and carbon.

The fluid temperatures at the time of carbonate precipitation were estimated using the isotope fractionation–temperature equation for the calcite–water system (O'Neil et al., 1969):

$$10^3 \ln\alpha_{\text{mineral–water}} = 2.78\ (10^6/T^2) - 2.89 \quad (1)$$

where α is the fractionation factor between mineral and water (the fluid); T is the fluid's temperature in Kelvin (K). The HCO_3^- state of carbon was assumed.

Sulphur isotope ratios ($^{34}S/^{32}S$) and oxygen isotope ratios ($^{18}O/^{16}O$) of pure $BaSO_4$ were analyzed in powders microdrilled from handpicked and cleaned barite samples following a procedure described in Giesemann et al. (1994) with a Thermo Finnigan Flash HT Plus elemental analyzer interfaced to a Thermo Scientific Delta V Plus mass-spectrometer. The samples were calibrated to $\delta^{34}S$ and $\delta^{18}O$ values of NBS 127 and IAEA-SO-6. Sulphur isotope values are reported as relative to the Vienna Canyon Diablo Troilite (VCDT) in terms of a $\delta^{34}S_{VCDT}$‰ and the sulphate oxygen isotope values are reported as relative to the Vienna Standard Mean Ocean Water (VSMOW) in terms of $\delta^{18}O$. The long–term reproducibility of the barite $\delta^{34}S$ and $\delta^{18}O$ measurements was better than ±0.3‰.

The fluid temperatures at the time of barite precipitation were estimated using the isotope fractionation–temperature equation (2) (Kusakabe and Robinson 1977):

$$10^3 \ln\alpha_{\text{mineral–water}} = 2.64\ (10^6/T^2) - 5.3 \quad (2)$$

The measurements of Sr isotope values of selected samples were carried out at the SGIker-Geochronology and Isotopic Geochemistry facility of the University of the Basque Country UPV/EHU (Spain). For these analyses approximately 100 mg of finely ground material was leached overnight in Teflon PFA vessels using 6N HCl at 100 °C. The solution was evaporated and the residue dissolved in 2.5 N HCl. Chemical procedures for sample treatment and Sr isolation followed those described in (Pin and Bassin, 1992). $^{87}Sr/^{86}Sr$ ratios were measured using a high-resolution Thermo Fisher Scientific Neptune Multi Collector Inductively Coupled Plasma Mass Spectrometer (MC-ICP-MS) in static multicollection mode, and corrected for mass fractionation by normalization to $^{88}Sr/^{86}Sr = 8.375209$ (Steiger and Jäger, 1977). The average $^{88}Sr/^{86}Sr$ ratio of NBS-987 standard over the period of analyses was 0.710264±0.000006. Strontium content in Sr-isotope samples was measured in the same powders dissolved in aqueous sodium carbonate (Markovic et al., 2016).

Fluid inclusion microthermometry was performed on doubly polished thick sections of calcite and sphalerite crystal aggregates using a Linkam THG600 heating-freezing stage. The shape of the inclusions varied considerably, and the criteria in Roedder (1984) were used to detect and avoid secondary inclusions.

The homogenization and final ice-melting temperatures were measured. Homogenization temperatures (Th) represent minimum trapping temperatures. Final ice-melting temperatures (Tm) provide an approximate measure of fluid salinity, which was estimated using the FLUIDS 1 code (Bakker, 2003). The stage was calibrated with synthetic standards for temperatures of −56.6 °C, −21.2 °C, −10.1 °C, 0.0 °C, 9.9 °C and 374.0 °C. The precisions of the measurements were estimated to be ±0.1°C at 0.0 °C and ±1° C at 374 °C. The compositions of the fluid and vapour phases in selected sphalerite fluid inclusions were determined by Raman micro-spectroscopy at the National University of Ireland, Galway using a Horiba LabRam II Raman spectrometer.

4. RESULTS

4.1. Calcite-sphalerite veins

4.1.1. Petrography and mineralogy

At least five thin, calcite-sphalerite bearing veins have been identified in the Kalana quarry. The veins are steep, vertical to sub-vertical (dips greater than 80°) and strike NE–SW or ENE–WSW. The veins have traceable lengths of greater than tens of metres and typically have thicknesses of 0.5–3 cm but reach up to 5–7 cm in some places. The veins are typically irregular (wavy) and in places are branching or stepping (Figures 2 and 3).

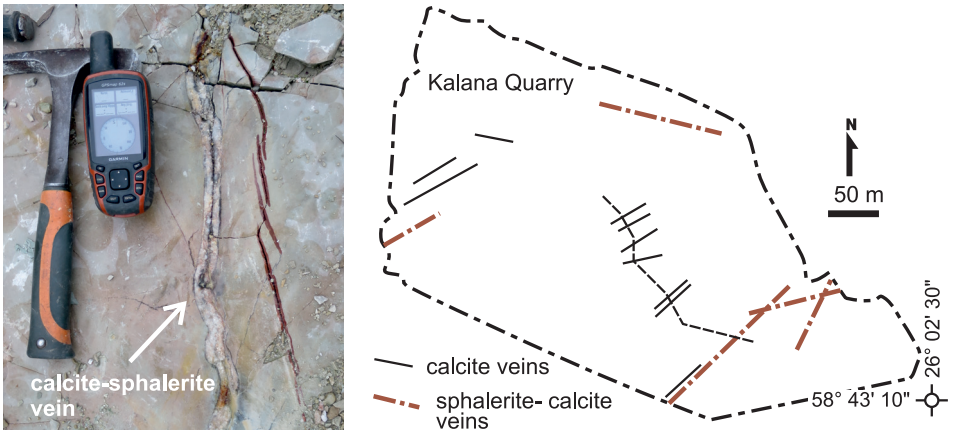

Figure 2. Photograph of the calcite–sphalerite vein in the quarry floor in Kalana and the location of calcite and calcite–sphalerite veins/fractures. (from Eensaar et al., 2017a – PAPER I)

The fillings of the veins show single-event syntaxial growth with full to partial sealing of the veins made up of blocky to elongate-blocky calcite aggregates. The XRD measurements of the microdrilled samples and the XRF and SEM-EDS mappings of the vein minerals (Figures 4, 5 and 6 in Eensaar et al., 2017a – PAPER I) show that sphalerite occurs primarily in the widened central parts of the calcite-filled veins and forms lens-like aggregates composed of c. 50–250 micron size crystals. However, the sphalerite and pyrite crystals are also found nucleating on vein walls preceding calcite crystallization (Figure 6 in Eensaar et al., 2017a – PAPER I). Rarely euhedral galena crystals are found in dolomitized host rocks next to calcite-sphalerite veins.

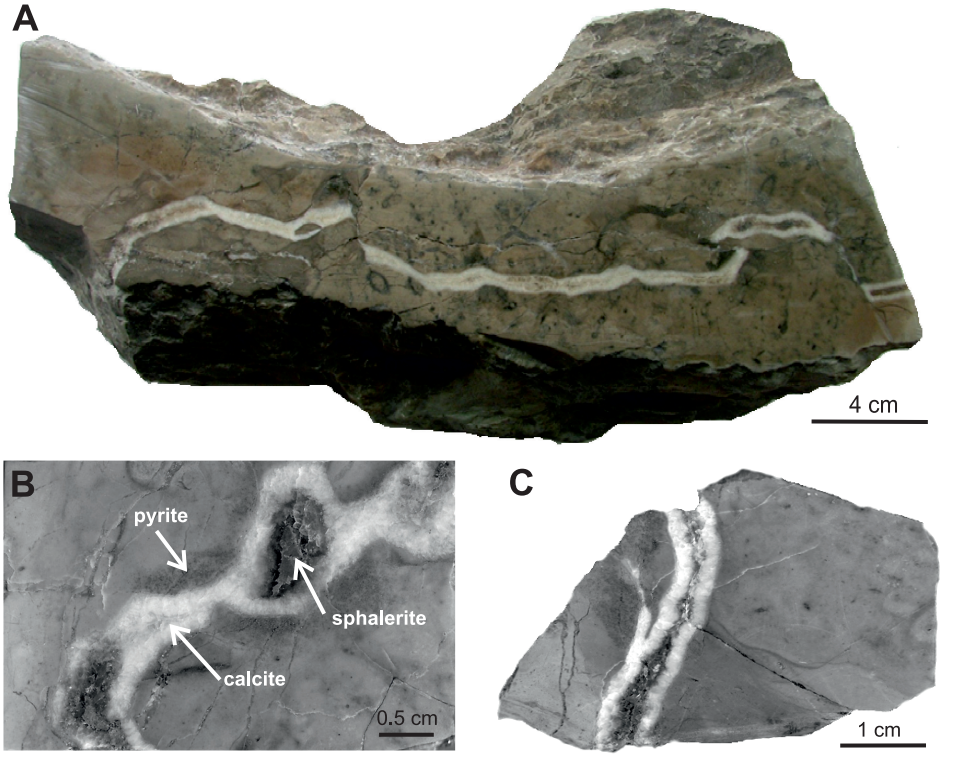

Figure 3. Photograph of a branching and stepping calcite–sphalerite vein in a block cut perpendicular to subvertical vein (A), close-ups of sphalerite aggregates in mineralized veins (B, C). (Eensaar et al., 2017a – PAPER I).

The mineralization paragenesis at Kalana is similar to the mineral association types in the Ordovician-Silurian carbonate sequences described by Palmre (1967) elsewhere in central and northeastern Estonia, characterized by pyrite–calcite–sphalerite/galena and pyrite–chalcopyrite/sphalerite/galena–calcite associations. The veins at Kalana are commonly bordered with finely dispersed pyrite mineralization "halos" that extend a maximum of 1–2 cm into the wallrock. However, the dolomitization of the wallrocks is patchy in appearance and does not show any preferential relationship to the calcite-sphalerite veins, although in some cases the fracture walls are encrusted by 10–100 μm thick dolomite bands.

4.1.2. Stable isotope composition of vein calcite

The $\delta^{13}C$ and $\delta^{18}O$ values of the wall-rock limestone and dolomite range from 0.3 to –3.2‰ and –3.6 to –6.7‰, respectively, which are similar to the stable isotope compositions of the Silurian period carbonate rocks in the Baltic Basin (Kaljo and Martma, 2000). The vein calcites show a range of $\delta^{13}C$ values from −1.7 to −6.8‰ and $\delta^{18}O$ values from −5.1 to −12.1‰, and show a negative trend

on a $\delta^{18}O$ vs $\delta^{13}C$ plot (Figure 4). More ^{18}O depleted calcite is observed at the contacts with the wall rock, and the $\delta^{18}O$ values increase and $\delta^{13}C$ values decrease toward the central parts of the vein.

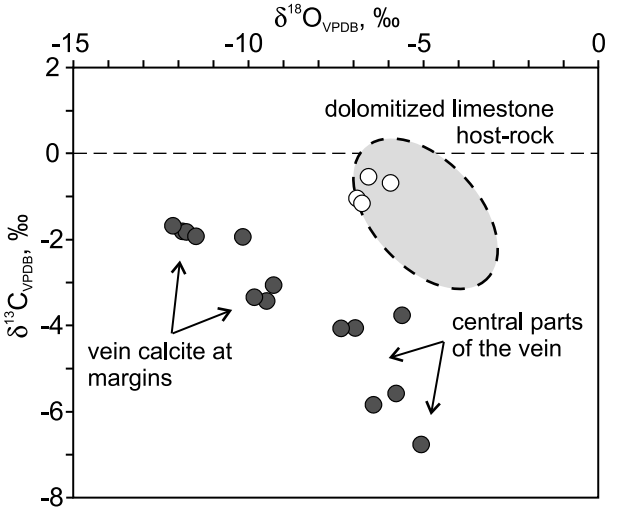

Figure 4. Cross-plot of $\delta^{18}O$ and $\delta^{13}C$ values of calcite in calcite–sphalerite veins and the host rock (dolomitized limestones). The shaded area shows the variation of the host rock composition. (from Eensaar et al., 2017a – PAPER I)

4.1.3. Fluid inclusions

Three fluid inclusion types were identified in the calcite in the calcite-sphalerite veins: (1) two-phase liquid-vapour inclusions with an approximately 90–95 volume % (vol %) liquid at room temperature; (2) mono phase liquid inclusions; and (3) rare liquid-vapour inclusions with a euhedral (rhombic?) solid phase.

The two-phase liquid-vapour fluid inclusions are most abundant in all of the samples but are predominantly small (commonly <5 μm) and/or secondary and deformed and therefore not suitable for microthermometric analysis. A few fluid inclusions suitable for analysis were found in only a single sample of vein calcite (KL09). The measured homogenization temperatures (Th) of these calcite-hosted fluid inclusions varie between 183 and 201 °C. The eutectic temperature (Te) of the fluid inclusions in the calcite is −21.2 °C, which suggests a H_2O-NaCl type solution (Borisenko, 1977). The last ice melting temperatures (Tlm) range from −1.1 to −2 °C, which suggests salinities between 2–3.5 wt% NaCleq (Bodnar, 1993).

In the sphalerite in the calcite-sphalerite veins at Kalana, two types of fluid inclusions were found: (1) primary two-phase liquid-vapour inclusions (Figure 8 in Eensaar et al., 2017a – PAPER I) and (2) secondary monophase liquid inclusions with the liquid phase filling at room temperature. The fluid inclusions are typically 30 to 100 μm and have a negative crystal shape. The primary

inclusions in the sphalerite show a degree of fill equal to 0.95–0.99. The measured Th values of the sphalerite crystals sampled from the aggregates in the central part of the calcite-sphalerite veins cluster at 60–85 °C and 90–120 °C, whereas the fluid inclusions of the few minute sphalerite crystals of the first generation sampled at the vein margins show homogenization temperatures between 192 and 200 °C (Figure 5). The derived values are minimum fluid trapping temperatures because the overburden at the time of sphalerite mineralization is unknown and so a pressure correction cannot be applied.

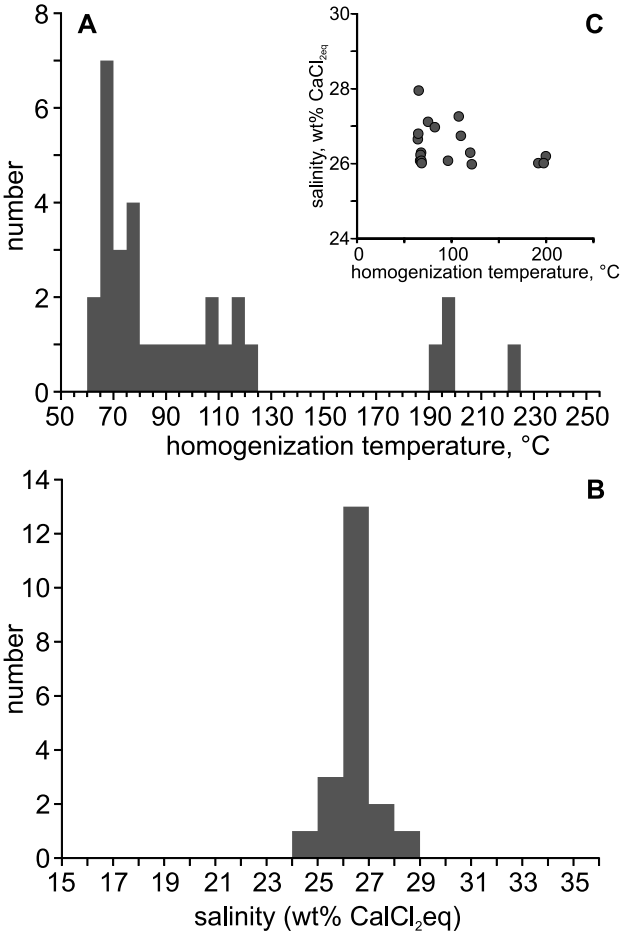

Figure 5. Homogenization temperatures (A), equivalent salinities (B) and homogenization temperature and salinity crossplot (C) of two-phase primary inclusions in studied sphalerite samples in Kalana. The homogenization temperature values are minimum temperatures because the pressure correction was not applied. (Eensaar et al., 2017a – PAPER I)

In contrast to the calcite-hosted fluid inclusions, using the sequential heating-freezing method, the two-phase sphalerite inclusions yield a mean temperature of first melting (Tfm) at −64.3 °C whereas hydrohalite formation-melting was not observed, which suggests the strong predominance of $CaCl_2$ among the solutes in the primary fluid. The Tlm values vary between −33.7 to −37.2 °C, which indicates high salinities of the fluids ranging from 24.3 to 27.9 wt% $CaCl_2$eq (Oakes et al., 1990) whereas there is no clear trend between salinities and trapping temperatures. The high salinities of the fluids are further confirmed by the skewness of the Raman O-H stretching band due to the water-chloride interaction in the liquid phase, which suggests that the salinities in the sphalerite fluid inclusions vary between 13–25 wt% NaCleq, according to the equation proposed by Mernagh and Wilde (1989).

4.2. Speleothem-like precipitates

4.2.1. Petrography

The fractures widened by karst-like processes and filled with botryoidal calcite and barite-pyrite aggregates constitute small caves that stretch along the preexisting fractures (Eensaar et al. 2017b – PAPER II). Calcite-barite filled vein crosscutting a thin undulating calcite-sphalerite mineralized vein in north-eastern part of quarry suggest that the latter postdate the sphalerite mineralization. The authigenic calcite crystals in dolomitized limestone cave walls of Kalana quarry have diverse shapes (equant-blocky, bladed and fibrous). In most part the cave walls are covered by an up to 10 cm thick speleothem crust of fine-crystalline calcite (Figures 2 and 3 in Eensaar et al., 2017b – PAPER II). The outer part of the crust is covered by centimetre-sized botryoidal (mammalies) calcite speleothems (Figure 6).

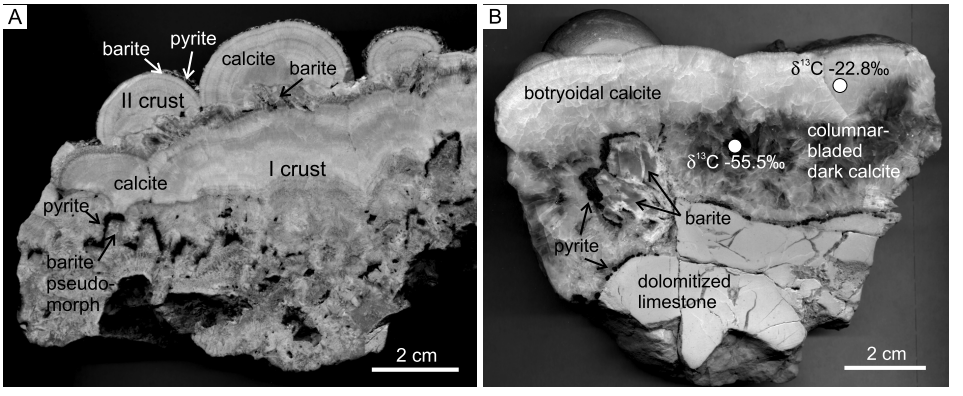

Figure 6. (A) Cross section of the botryoidal crust showing the cyclic character of barite–pyrite and calcite precipitation; (B) paragenetic relationships of phases and variation in the measured calcite $\delta^{13}C$ values (white dots indicate the location of microdrilled samples) (from Eensaar et al., 2017b – PAPER II).

The paragenetic sequence of the cave/fracture wall precipitates starts with sparsely placed bladed-euhedral (rhombic) barite crystal aggregates of the first generation (Figure 7). The barite crystal aggregates are nucleated at the limestone-dolomite wall-rock and on some occasions the barite aggregates show a macroscopically dendritic growth pattern.

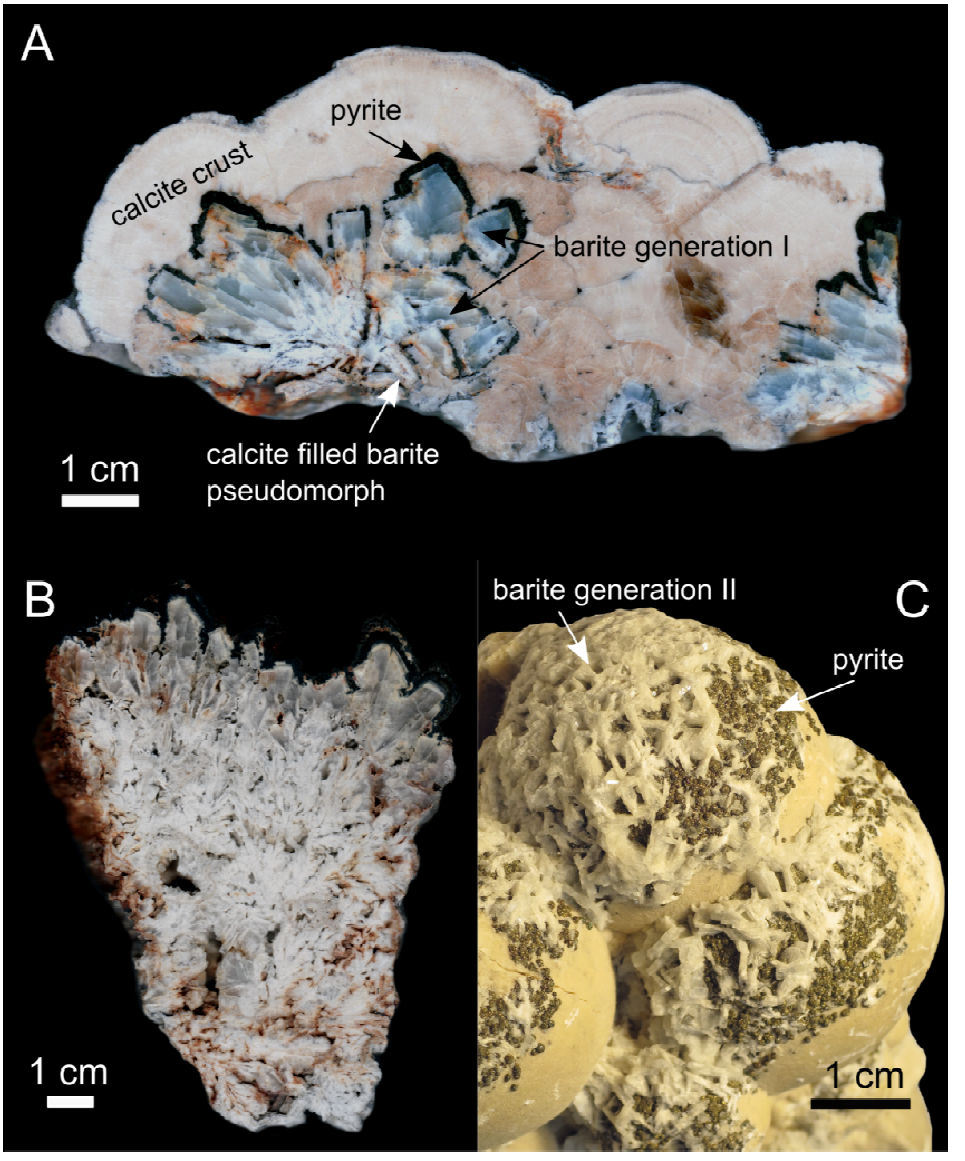

Figure 7. Cross section of the botryoidal crust showing the cyclic character of barite–pyrite–calcite–barite–(pyrite) precipitation (A); cross section of dendritic barite aggregate (B) and barite generation II growing on calcite botryoidal aggregate (C). (Gaškov et al., 2017 – PAPER III)

Barite crystals growing in the fractures and the wall rocks are frequently encrusted with a 1–4 mm thick layer of microcrystalline pyrite aggregates. In cave walls these aggregates are all covered by curved-face columnar-bladed calcite showing sweeping extinction and grading into finely laminated calcite aggregate. Laminated calcite aggregates form botryoidal surfaces that coalesce into distinct layers. About 0.3–2.5 mm thick laminae are composed of epitaxially overgrown acicular/thin bladed calcite crystals oriented perpendicular to the layering. Sequences of laminated botryoidal calcite occur in at least three repeated cycles. The succeeding cycle is built by sparsely spaced small mammalies nucleated at these boundaries and coalescing into the next layer. The columnar-bladed calcite in the central parts of the botryoidal aggregates and margins of coalescing mammalies have brownish-dark colouring caused by abundant impurities and microscopic gas–fluid inclusions (Figure 4 in Eensaar et al., 2017b – PAPER II).

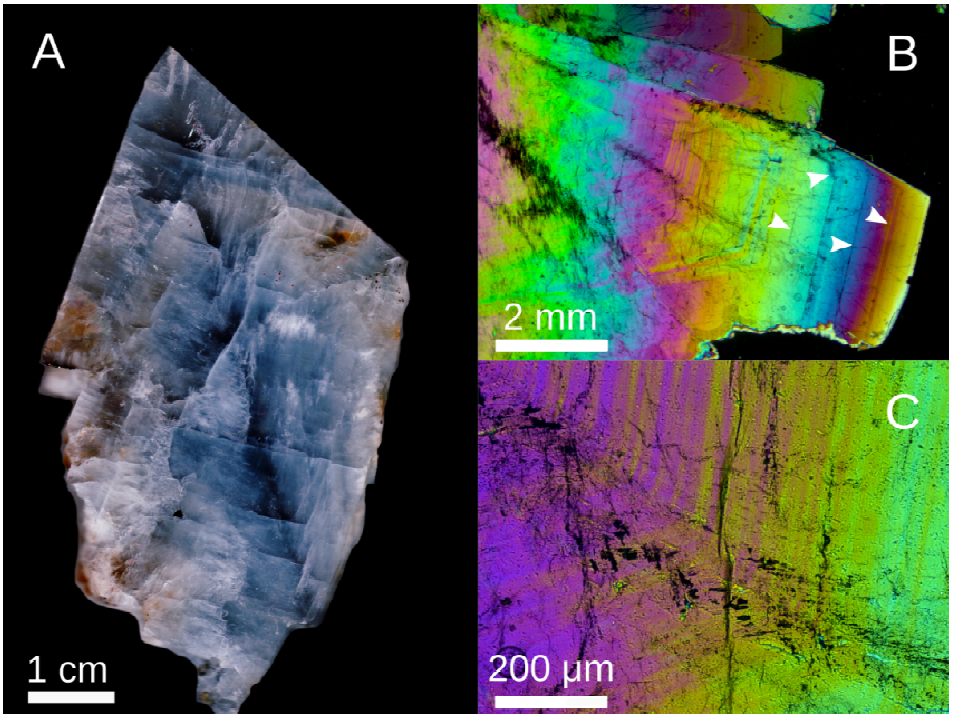

Figure 8. Cross section of a tabular barite crystal showing macroscopic growth banding (A); microphotographs of growth bands under polarizing microscope in crossed polars, arrows indicate wider growth bands in outer parts of the crystal (B); fine growth bands in the central part of the zoned crystal (C). (from Gaškov et al. 2017 – PAPER III)

The boundaries of the cycles are marked by a thin layer of bladed calcite and occasionally covered by sparse aggregates of thin-bladed barite of the second generation and/or pyrite. The second generation of barite occurs typically as a few mm thick and up to 1 cm in width/length, pale-grey to white tabular crystals on the surfaces of laminated botryoidal calcite aggregates.

The size of the pale blue to transparent barite crystals of the first generation reaches up to 7 cm in length, 5 cm in width and up to 1–1.5 cm in thickness. Individual barite crystals cut along the long axis show zonal colouring typically from dark blue – pale blue/transparent – dark blue. Under a polarizing microscope (Figure 8) the barite crystals show distinct growth bands that are few to tens of μm wide in the central parts of the crystal aggregates and grow wider (up to several mm in width) in the outer portions of the crystals.

In some cases the barite at the base of botryoidal calcite aggregates has been intensely leached to white opaque microcrystalline calcitic masses. This leaching antedated the deposition of the botryoidal calcite in which the barite blades are embedded. The replacement of barite suggests varying oxidizing and reducing conditions as the barite is readily destroyed in reducing environments (Hanor, 2000).

4.2.2. Mineralogy and mineral chemistry

X-ray diffraction analysis of calcite precipitates shows that different types of calcite in the studied speleothem samples are represented by low-Mg calcite with less than 3 mol% $MgCO_3$. However, Mg content is up to 3880 ppm in columnar-bladed calcite and 450–990 ppm in finely laminated botryoidal calcite. Strontium content in speleothem calcite ranges from 60 to 720 ppm, being somewhat higher in laminated botryoidal crusts. Barium content is 60–260 ppm in the laminated crusts/mamelons and 60–80 ppm in the bladed crystal aggregates in the lower part of the crust. The Fe and Mn contents of different calcite types are 200–630 ppm and 150–740 ppm, respectively.

The composition of barite is close to stoichiometric with little variation in unit cell parameters suggesting a less than 5 mol% of $SrSO_4$ substitution in the barite at Kalana, 2–4 mol% of $SrSO_4$ according to Goldish (1989). This is in accord with 0.1–1.6 wt% of Sr measured in barite crystals. However, Sr content in barite crystals shows variation with respect to the growth zones and the barite generations. Minute barite crystals of the second generation are characterized by Sr content typically less than 0.2 wt%. In the zonal crystals of the first generation, the central parts of the crystal aggregates show elevated Sr (up to 1.6 wt%) whereas Sr is progressively depleted in the outer zones of the larger crystals and the outermost growth zones have commonly Sr contents less than 0.3 wt%. SEM microprobe analysis of the fine growth zones within individual barite crystals indicates that Sr is higher in the darker zones and lower in bright zones (Figures 3 and 4 in Gaškov et al. 2017 – PAPER II).

4.2.3. Stable isotope composition

Stable carbon and oxygen isotopes of wall-rock limestone and dolomite in Kalana sequence show values typical to normal marine carbonates and range from 0.3 to –3.2‰ and –3.6 to –5.3‰, respectively (Figure 9). The speleothem calcites, however, show extreme depletion in ^{13}C and large variations in $\delta^{13}C$ values from −11.6 to −55.9‰, while $\delta^{18}O$ values range from −4.5 to −11.4‰). Some of the wall-rocks sampled close to the cave/fracture surface are also depleted in ^{18}O and have slightly lower $\delta^{13}C$ values. The $\delta^{13}C$ values decrease towards the early growth stages of the botryoidal crusts, whereas the strongest ^{13}C depletion was measured in the dark-brownish columnar-bladed calcite (Figures 3 and 5 in Eensaar et al., 2017b – PAPER II).

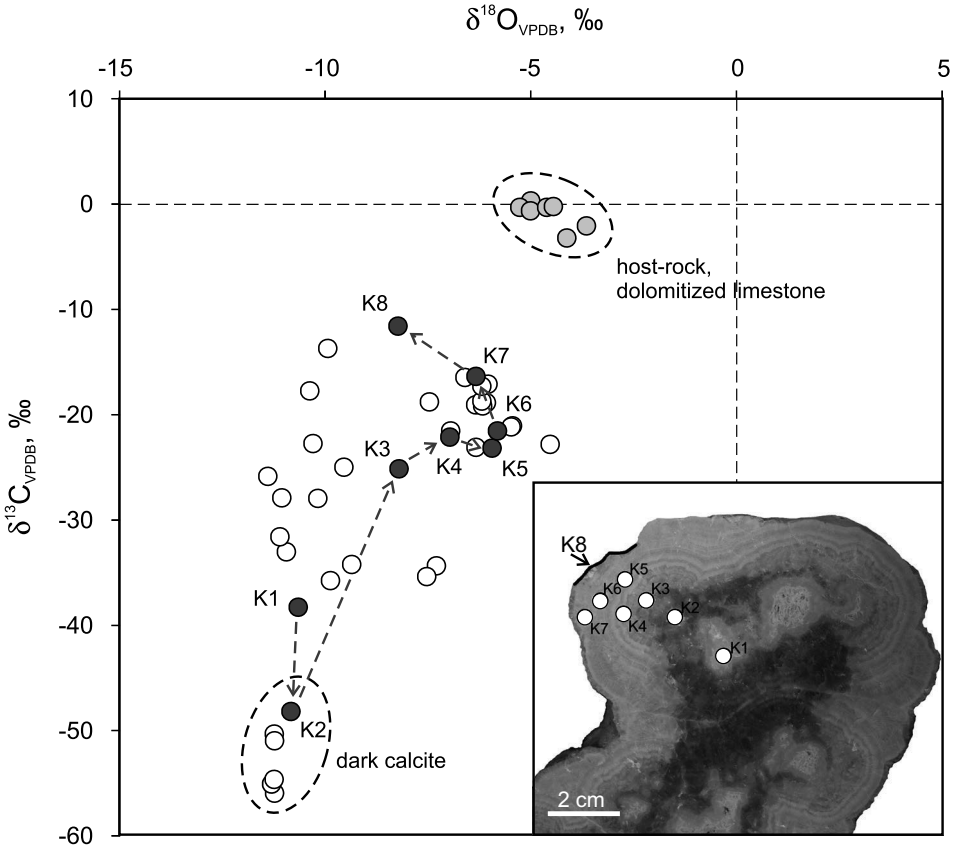

Figure 9. Cross-plot of $\delta^{18}O$ and $\delta^{13}C$ values in authigenic calcite from the cave and the host rock (dolomitized limestones).(Eensaar et al., 2017b – PAPER II).

Sr-isotope ratios in the barite sampled in Kalana vary narrowly from 0.711410 to 0.712033 whereas the sulphur isotope composition of the studied barite samples ranges from 13‰ to 33‰ (Figures 5 and 6 in Gaškov et al., 2017 – PAPER III). The $\delta^{34}S$ values of different barite generations overlap. The $\delta^{34}S$

values, however, show systematic variation in large, zonal barite crystals. The lowermost $\delta^{34}S$ values (<16‰) are found in the central parts of the crystals and the $\delta^{34}S$ values increase towards the edges, reaching up to 33‰ (Figure 10). Isotope composition of the oxygen in barite varies typically between 15‰ to 19‰ and differently from the sulphur isotope composition the sulphate $\delta^{18}O$ values do not show systematic variation with respect to the growth zones in the larger crystals. Only a few samples of the barite show ^{18}O enriched composition with $\delta^{18}O$ values higher than 20‰.

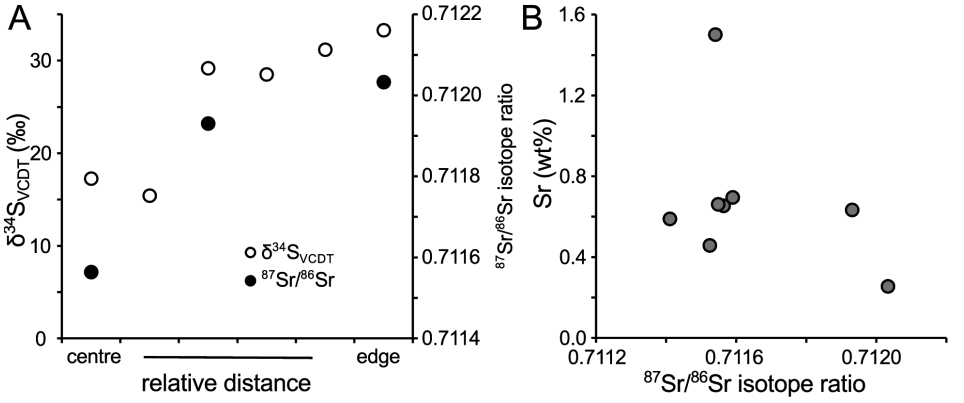

Figure 10. Variation in Sr isotope ratios and sulphate $\delta^{34}S_{VCDT}$ values in a single crystal of generation I (A); cross-plot of $^{87}Sr/^{86}Sr$ ratios and Sr concentrations (B). (Gaškov et al. 2017 – PAPER III)

5. DISCUSSION

This study shows evidence of hydrothermal fluid activity in fracture zones that intersect a Silurian carbonate sequence in Kalana, central Estonia, in the northern part of the Baltic palaeobasin. The fluidal activity is characterized by an earlier low- to moderate temperature hydrothermal mineralization phase resulting in calcite-sphalerite veins and a later and possibly a separate fluid activity event characterized by low temperature (warm) fluids running in the same fracture systems and responsible for widening the existing fractures/veins and precipitation of calcitic speleothem-like aggregates, spar calcite, barite and pyrite in repeating cycles.

5.1. Hydrothermal veins

The petrography of the calcite-sphalerite vein fillings suggests a syntaxial growth from a fluid with elevated temperatures, whereas the sphalerite (pyrite) and calcite deposition occurred in several stages.

Northern part of the Baltic paleobasin has been traditionally considered to be devoid of any major tectonic disturbances and/or magmatic activity since the Palaeozoic although Early Carboniferous (351 ± 11 Ma) dolerite intrusions are reported in the southern part of the basin in the Baltic Sea off the coast of Lithuania that were possibly emplaced in relation to the northwest ward prolongation of the 370–359 Ma Pripyat–Dnieper–Donetsk Rift (Motuza et al., 2015). However, in the shallowly buried central-northern part of the basin in Estonia and Latvia, the last recorded large scale magmatic episode was the emplacement of c. 600 Ma foidic basalt flows in Latvia (Brangulis, 1985).

The modern heat flow in the basin, which is situated in the interior part of a 1.8–1.9 Ga old craton, is only 50 mW m^{-2}, and deep seismic profiling of the c. 110 km thick lithosphere indicates no major tectonic activity in the Phanerozoic, which suggests that the thermal gradients in the interior of the basin could not have been much higher in Phanerozoic times (Kukkonen and Jõeleht, 2003). Most of the faults identified in the sedimentary cover in the northern part of the basin have southwest-northeast orientations, typically vertical displacements less than 50 m and are interpreted to have formed under the northwest-southeast compressional regime along the Caledonian front during the Baltica and Laurentia collision in the Silurian–Devonian (Šliaupa et al., 2000).

There is abundant evidence of hydrothermal fluid activity and Pb-Zn mineralization in relation to the Caledonian orogeny at the Caledonian front as well as in east-central Sweden, in an area next to the Baltic palaeobasin. The mineralization of the regionally hosted, extensive fracture-controlled crystalline basement and Cambrian sandstone impregnation-type, world-class Pb-Zn deposits along the Caledonian front are suggested to have occurred during the final Scandian phase of the Caledonian orogeny between 430 and 400 Ma

(Billstrom et al., 2012; Rickard et al., 1979). Recently, Saintilan et al. (2015) suggested, relying on a sphalerite Rb-Sr age of 467 ± 5 Ma in the Laisvall sandstone-hosted Pb-Zn deposit, Sweden, that its formation was a response to early Caledonian orogenic activity. The in situ Ar/Ar dating of authigenic K-feldspar in the Pb-Zn host sandstones of Neoproterozoic – Lower Cambrian Såvvovare Formation of the Laisvall Group, Northern Sweden, suggests two separate events of K-feldspar growth – an early diagenetic event at 528–567 Ma and a tectonically induced fluid flow event at 425–400 Ma, which was possibly related to the collapse of the Caledonian orogen (Sherlock et al., 2005).

Similarly, Caledonian ages of mineralization are suggested by Pb/Pb, U/Pb and Nd model ages of calcite, fluorite and galena veins in east-central Sweden and southern Finland (Alm et al., 2005). Mineral, fluid and isotope studies of fracture-controlled mineralization in the crystalline basement of central Sweden indicate several mineralization events (Drake and Tullborg, 2009; Drake et al., 2009; Sandström and Tullborg, 2009; Sandström et al., 2006; Sandström et al., 2009). The two oldest events are linked to the Proterozoic development of the craton, the third mineralization event, which was characterized by mineralization at temperatures of 60 to 190 °C, was explained by mixing of diagenetic and deep crystalline bedrock fluids that was probably a far-field response to the Caledonian orogeny and/or the development of the Caledonian foreland basin (Sandström and Tullborg, 2009). The same event is possibly recorded in calcite-filled veins in southwestern Finland (Sahlstedt et al., 2010; Sahlstedt et al., 2013). The fourth event described in Sweden is related to episodic calcite precipitation at temperatures <50 °C during the long period from the Late Palaeozoic to the present (Drake et al., 2009).

Paleomagnetic studies of dolomitized Silurian carbonate rocks and Cambrian to Lower Ordovician siliciclastic rocks in the northern Baltic palaeobasin as well as in southern Finland point to three major remagnetization events (Plado et al., 2010; Plado et al., 2008; Preeden et al., 2009; Preeden et al., 2008):

(1) Silurian – early Devonian,

(2) late Devonian – Carboniferous (Mississippian) and

(3) late Palaeozoic (Permian) – Triassic overprinting.

The first and second events are carried mainly by magnetite, and (titano)hematite/ maghemite in the third event (Khramov and Iosifidi, 2009; Plado et al., 2008; Preeden et al., 2008).

Also, a fourth remanent magnetization component associated with Mesozoic (Jurassic – Cretaceous) remagnetization has been revealed in some Silurian sections in Estonia, in Devonian dolostones in Latvia and in Ordovician limestones in northwestern Russia. This is, however, carried by hematite and goethite which points to shallow and oxygenated fluids during the Mesozoic event (Katinas and Nawrocki, 2004; Plado et al., 2008; Smethurst et al., 1998), and is not consistent with the chemical conditions required for sulphidic mineralization.

Similarly, the late Paleozoic (Permian) to Triassic remagnetization is rather well recognized in both Silurian and Ordovician carbonate rocks and in Cambrian to Lower Ordovician sandstones in Estonia and northwestern Russia, and it is carried by, as suggested from isothermal remanent magnetization behaviour, (titano-)hematite and/or maghemite, which likely indicates near-surface alteration by meteoric fluids (Khramov and Iosifidi, 2009; Plado et al., 2008; Preeden et al., 2008). The uplift in the Baltic palaeobasin was linked to thermal doming during the Carboniferous to Permian (Šliaupa and Hoth, 2011) and caused disappearance of the sedimentary basin in the Baltic region (Usaityte, 2000) exposing the sedimentary successions to continental oxidising conditions and erosion.

The sulphidic hydrothermal mineralization in central Estonia can then be viewed within this context as a southeastward continuation of the Caledonian mineralization event similar to that in Scandinavia rather than associated with late Palaeozoic or Mesozoic diagenetic events. Presence of a Caledonian-related fluid-event is in the northern Baltic palaeobasin further supported by a late Silurian–Devonian K-Ar age of the illitization (Somelar et al., 2010) and remagnetization overprint in Silurian carbonate rocks carried by magnetite (Preeden et al., 2008). However, it is important to note that, in central Estonia and in Latvia, the fracture-controlled sulphidic mineralization extends up to the lower part of the Middle Devonian (Eifelian, 393.3–382.7 Ma) dolomite-domerite sequence of the Narva Regional Stage (Fedorenko and Menaker, 1977; Palmre, 1967; Pichugin et al., 1976). This indicates that the maximum age of mineralization is somewhat younger (c. 5–20 million years) than that of the Pb-Zn ores at the Caledonian front. This age difference between the hydrothermal activity in Scandinavia and in the Baltic palaeobasin is also evident from K-Ar ages of mixed-layer minerals in bentonites, which suggests an illitization event in the northern part of the Baltic palaeobasin at 370–400 Ma (Somelar et al., 2010; Somelar et al., 2009). A slightly younger age (c. 380 Ma) is also observed for the Sm-Nd ages of hydrothermal fluorite- and galena-bearing veins in southern Finland (Alm et al., 2005). Moreover, Högdahl et al. (2001) have suggested that the resetting of U-rich zircons to the east of the Caledonian front that resulted in discordant ages of 384 ± 15 Ma was caused by flushing of c. 150 °C saline fluids. This suggests that the duration of the Caledonian hydrothermal activity in Fennoscandia was possibly not limited to the end of the Scandian phase at approximately 400 Ma. The minimum age of the mineralization in northern Baltic palaeobasin is, at present state of knowledge, somewhat arbitrary and needs further study (e.g., direct Rb-Sr dating of sphalerite), but could be placed in late Devonian – Carboniferous as suggested by the paleomagnetic data (Plado et al., 2008).

The similarities of the Scandinavian Pb-Zn mineralization and fracture-controlled calcite-sphalerite(galena) veins in central to northwestern Estonian and other Pb-Zn mineralization occurrences in Estonia, including impregnation-type mineralization in Ediacaran sandstones in northern Estonia, are further supported by the mineral associations and paragenesis of the deposits and, more

importantly, by the properties of the mineralizing fluids. The sphalerite-precipitating fluids at Kalana were characterized by rather low minimum trapping temperatures (65–200 °C) and NaCl-$CaCl_2$-H2O compositions with medium to high salinities (10–30 wt% $CaCl_2$eq). A few measured homogenization temperatures of 180–200 °C in calcite-hosted fluid inclusions, though suggesting considerably lower salinity, coincide with the higher limit of the sphalerite-hosted inclusions. The negative trend of the $\delta^{18}O$ and $\delta^{13}C$ values of the vein calcite (Figure 7 in Eensaar et al., 2017a – PAPER I) can be explained by the mixing of two fluids (Zheng and Hoefs, 1993) – a shallow low temperature (<50 °C) fluid with a dissolved inorganic carbon (DIC) $\delta^{13}C$ value of –1‰ and $\delta^{18}O_{SMOW}$ value of 0‰, and another, possibly deep and high temperature (>150 °C) hydrothermal fluid, characterized by a DIC $\delta^{13}C$ value of –10‰ and a $\delta^{18}O_{SMOW}$ value of 13‰.

Similarly, the sphalerite-hosted fluid inclusion homogenization temperatures in the fracture-controlled and/or sandstone-hosted Pb-Zn ores at the Caledonian front show homogenization temperatures ranging from <70 to 182 °C (maximum 220 °C) and salinities of the NaCl-$CaCl_2$-H_2O fluid between 14–24 wt% NaCl-$CaCl_2$eq (Billstrom et al., 2012; Kendrick et al., 2005; Lindblom, 1986; Rickard and Lindblom, 1979).

The mineralization style and fluid characteristics of these Pb-Zn occurrences in Scandinavia and in the northern Baltic palaeobasin are remarkably similar to Mississippi Valley Type (MVT) ores worldwide (Leach et al., 2010). On the other hand, Kendrick et al. (2005) have shown that despite these similarities the Scandinavian Pb-Zn deposits probably represent a false analogue for the MVT ore districts, mainly because of its different tectonic setting at the deformational front of the Caledonian orogeny, rather than in association with a foreland basin, which is characteristic (Leach et al., 2010). Instead, the sulphide mineralization described in the northern part of the Baltic palaeobasin, including the mineralization in the Silurian carbonates at the Kalana quarry, could represent an epigenetic sediment-hosted Pb-Zn mineralization of an MVT subtype (Leach et al., 2010). Firstly, it is hosted by dolostone-limestone in a platform carbonate sequence. Secondly, it is placed in a passive margin setting of the Baltica continent facing the Caledonides, which were uplifted in the Baltica-Laurentia collision. Thirdly, the mineral association is represented by sphalerite-galena-pyrite deposited from low temperature and moderate-high saline NaCl-$CaCl_2$ dominated fluids.

Based on flexural subsidence and thermal modelling, Middleton et al. (1996) suggested a foreland basin up to 6 km deep in front of a Himalayan-type Caledonian orogeny with the forebulge axis running along the present-day Gulf of Bothnia. Several AFT model compilations (Murrell and Andriessen, 2004) have suggested that the burial of the sub-Cambrian peneplain at 4–6 km depth in Scandinavia caused a significant reheating event.

The existence of a deep foreland basin at the Caledonian front has been challenged (Hendriks et al., 2007b; Hendriks and Redfield, 2005a; Hendriks and Redfield, 2005b) showing that there is no direct evidence for a deep and

extensive foreland basin, at least at the eastern margins of Fennoscandia. However, during the Silurian, the northern part of the Baltic palaeobasin was gradually uplifted and completely emerged by the end of the Silurian, at c. 416 Ma (Nestor and Einasto, 1997). This coincides with the most intensive uplift phase of the Caledonides c. 420 Ma (Milnes, 1998), and indicates the development of a migrating forebulge in the foreland of the Scandinavian Caledonides. Additionally, the formation of synsedimentary, reversed compression or transpression, southwest-northeast oriented faults in the Baltic palaeobasin in the late Silurian to early Devonian (Lochkovian) coincides with this period (Poprawa et al., 1999) whereas the gentle folding and fracturing in Kalana could be interpreted as resulting of the same process.

These faults provided migration routes for fluids that could have been either meteoric waters percolating by gravity-driven flow at topographic highs within the collision zones or deep-seated basinal brines driven by tectonic compression and geothermal gradients away from the thrust zone(s) toward the foreland basin. It is also important that the cross-cutting relationships of the Pb-Zn mineralization in the northern part of the Baltic palaeobasin suggest that a mineralization event occurred in the early Middle Devonian, when the sedimentation in the northern part of the basin was resumed and continued until the infilling of the basin by the Late Devonian as the foreland basin was uplifted due to the extensional collapse of the Scandinavian Caledonides in Early Devonian Emsian times (Plink-Björklund and Björklund, 1999). In this sense, the sulphide mineralization in the northern part of the Baltic palaeobasin could be considered occurred as in a characteristic MVT foreland setting.

5.2. Formation of cave precipitates

Structural relationships between calcite/calcite-sphalerite veins and cave-like structures stretching along the fracture planes suggest that cave structures are developed by widening of few to tens of centimeters wide fractures by karst-forming processes (Eensaar et al. 2017b – PAPER II). Most of the cave-like structures (typically small – up to 0.5–1 m wide, up to 15 m long and the widened parts 1.5 m in height) are found in the central and southern parts of the quarry in sub-vertical contact zones between limestone and dolomite bodies, in an about 2 m high zone at the base of the 10–15 m high quarry wall, whereas the fractures and veins run typically in full height of the exposed section. Widened parts of fractures are rarely found in upper part of the section.

The occurrence of cave-like structures at the same level all over the quarry suggest either some lithological control over their formation and/or the depth of a zone with environmental conditions favorable for carbonate rock dissolution and cave formation. There is no indication of prolonged aerial exposure (sedimentary hiatuses) at this level (Männik et al., 2016) but the cave structures are located in the interval where dolomitized limestones (wackestone and/or packstone) with thin lenses and irregular interbeds of light to dark brown

organic-rich microlaminated dolomitized argillaceous limestone are capped by a beds of cross-bedded recrystallized and hard fine-grained carbonate grainstone with a thickness of 1–4 m, then followed by partly dolomitized greenish-grey argillaceous micritic limestone occurring upwards. Cave structures occur only in the lower part of the section (wackestone and/or packstone limestone) and do not extend upwards into grainstone and/or argillaceous micritic limestone suggesting that grainstone-argillaceous limestone beds have acted as (semi-)impermeable shields controlling the fluid movement and development of cave structures.

5.2.1. Calcite precipitates

It is unusual to cave deposits/precipitates that analyses of the carbon isotopic composition of the speleothem calcite from Kalana yield $\delta^{13}C$ values generally lower than –15‰, reaching as low as –56‰ (Figure 5 in Eensaar et al., 2017b – PAPER II). In typical cave systems the carbon isotopic composition of a low-Mg calcite speleothem is mainly controlled by the carbon isotopic composition of dissolved inorganic carbon (DIC), given that the fractionation between DIC and the calcium carbonate precipitating in the system is small, and kinetic effects are negligible (Frisia et al., 2011; Romanek et al., 1992).

The main sources for the different DIC species in percolating water are soil CO_2 produced by root respiration, decomposition of organic matter and the dissolution of carbonate host rock, and atmospheric CO_2. Because of the nearly complete equilibration between soil CO_2 and dissolved bicarbonate (HCO_3^-), soil CO_2 dominates in speleothem carbon in an open system, but its estimated contribution would be c. 85 % if the flux of CO_2 through the vadose zone is not large enough (Genty et al., 1999). Soil CO_2 (assuming C3-dominated origin of organic matter) has a $\delta^{13}C$ value of –30 to –20‰ and, considering fractionation between CO_2 – bicarbonate – calcite (Breecker et al., 2012), speleothem calcite would display the ratios of –14 to –6‰ without a host-rock contribution (Cerling, 1984; McDermott, 2004).

The $\delta^{13}C$ values of dolomitized limestone bedrock in Kalana vary between –3.2 and 0.3‰ and taking a host-rock contribution of 15 % with an average $\delta^{13}C$ value of –1‰ into account, the speleothem calcite in Kalana should display $\delta^{13}C$ ratios between c. –13 and –5‰.

On the other hand, such ^{13}C depleted calcite is commonly encountered in modern and ancient carbonate precipitates at methane seeps (Campbell, 2006; Himmler et al., 2008; Natalicchio et al., 2012; Paull et al., 1992; Peckmann et al., 1999; Peckmann and Thiel, 2004; Roberts et al., 2010). The ^{13}C-depleted carbon source for the precipitation of authigenic seep carbonates is supplied by microbially mediated anaerobic oxidation (AOM) of hydrocarbons such as methane and oil (Boetius et al., 2000; Joye et al., 2010), typically within shallow subsurface sediments. At these settings the hydrocarbons rising through unconsolidated sediments are anaerobically oxidized at the lower boundary of the sulphate reduction zone either by microbial consortia of archaea producing CO_2 and water, and sulphate-reducing bacteria that convert sulphate to hydrogen

sulphide (HS^-) (Boetius et al., 2000; Orphan et al., 2002; Whiticar, 1999) or just by anaerobic methanotrophic archaea that oxidize methane and also produce disulphide (HS_2^-) (Milucka et al., 2012). Alternatively, AOM can be driven by nitrate dismutation and/or be coupled to metal-oxide reduction (Beal et al., 2009; Ettwig et al., 2010). All of these different modes of AOM increase pore-water alkalinity and consequently cause the precipitation of carbonates.

Carbon isotopic values in Kalana speleothems vary systematically, ranging from –35 to –56‰ in the dark-brownish columnar-bladed calcite in the lower/central part of the botryoidal crusts to progressively less ^{13}C depleted laminated calcite and the outermost thin columnar layer of the crust with $\delta^{13}C$ values –30 to – 20‰ and –12 to –9‰, respectively. This may reflect (a) the variation in the source of methane e.g. microbial vs. thermogenic origin, or (b) mixing of different sources into the DIC pool, e.g. dilution of microbial and thermogenic methane carbon by seawater DIC.

Microbial methane is formed in anaerobic conditions typically via CO_2 reduction and/or acetoclastic methanogenesis, whereas thermogenic methane is generated during organic matter maturation (Whiticar, 1999). Biogenic methane formed by methanogens is strongly depleted in ^{13}C and its $\delta^{13}C$ values vary from −110 to −50‰, typically −60 ± 5‰ (Sapart et al., 2012; Schoell, 1988). On the other hand, thermogenic methane is typically characterized by higher $\delta^{13}C$ values over –50‰, up to −22 ± 3‰ in pyrogenic methane (Sapart et al., 2012). In this sense the low $\delta^{13}C$ values of calcite precipitates in the centre of botryoidal crusts clearly indicate AOM-derived carbon dominating in the DIC pool from which the carbonate precipitated. However, the less depleted isotopic composition of carbon in paragenetically following laminated calcite may either reflect a change in the primarily thermogenic methane source or indicate the mixing of different sources into the DIC pool. Alternatively, assuming a closed DIC pool, the relative enrichment in calcite ^{13}C would reflect an isotopically heavier composition of the residual methane remaining after the biological consumption of the isotopically lighter fraction of the initial methane in methane-limited but sulphate-rich AOM (Yoshinaga et al., 2014).

The source and origin of methane in Kalana rocks are unknown. Unlike modern and fossil methane seep carbonates, precipitating or being precipitated at the (shallow) seafloor at passive continental margins via biogenic methane seeping through a soft, yet unconsolidated, organic-rich sediments, the ^{13}C-depleted carbonates in Kalana were precipitated in a cave–fracture system developed in lithified diagenetically recrystallized carbonate rocks. Deep-seated AOM activity, possibly driven by autoendolithic life (Marlow et al., 2015) and resulting in the precipitation of AOM-related ^{13}C-depleted carbonate phases, have been described in few case studies both in fractured crystalline and sedimentary rocks (Drake et al., 2015). In most cases the subsurface AOM is found in the transition zone of deep methane-carrying fluids and sulphate-rich surface water (Pedersen, 2013). However, a reversed system has been proposed for fractured granite in Sweden, where the most extremely ^{13}C-depleted calcite reached a $\delta^{13}C$ value of –125‰ (Drake et al., 2015).

Clayey carbonates rich in disseminated algal organics as well as complete algae fossils preserved in the lower part of the Aeronian rocks exposed in the Kalana section (Tinn et al., 2009), with a Corg content up to 3 wt% (Kalle Kirsimäe, unpublished data, 2014), could have been possible source rocks for methane. Thermogenic methane is produced by thermocatalytic degradation of kerogen at temperatures over 120 °C (Tissot and Welte, 1984). Considering the typical geothermal gradient in the old and tectonically stable cratonic Baltic paleobasin, c. 20 °C/km (Kirsimäe and Jorgensen, 2000), the formation of thermogenic methane would require burial depths greater than 3–4 km. This would contradict the immature state of organic matter (Talyzina, 1998) and uncompacted clayey sediments in the lower part of the Palaeozoic sedimentary sequence of the northern Baltic Basin. Shallow burial of the basin at its northern margin is also implied by apatite fission track ages of 500–800 Ma in crystalline basement rocks at the northern margin of the basin in southern Finland (Hendriks et al., 2007a), suggesting that the sequence has not been deeply buried and/or regionally heated up for the thermogenic methane production throughout the Phanerozoic. Nevertheless, the diagenetic grade of clay minerals and palaeomagnetic remagnetization of sediments hint at a series of basinwide (hydrothermal) fluid intrusions/thermal perturbations during the evolution of the Baltic Basin (Preeden et al., 2008; Somelar et al., 2010). The cave structures in Kalana developed along the fracture systems where hydrothermal fluids could have been capable of locally heating up the organic-rich sediments and thermogenic methane production. Nevertheless, although the AOM of thermogenic methane with $\delta^{13}C$ values between –20 and –50‰ (Sapart et al., 2012) could explain the isotopic composition of calcite precipitated in the outer part of the botryoidal speleothems, the most ^{13}C-depleted bladed-columnar calcite would have required the oxidation of biogenic methane as the source for carbon.

5.2.2. Origin of barite

Meteoric water as well as shallow groundwater in Estonia are low in dissolved sulphate (Raidla et al., 2014) and therefore do not represent a favourable fluid environment for sulphate-reducing bacteria anaerobically oxidizing methane. However, ^{13}C-depleted calcite speleothems in Kalana are associated with the precipitation of abundant pyrite and euhedral barite that specifically point to a fluid system rich in dissolved sulphur species.

Barite is known to form at sulphate–methane interfaces (Castellini et al., 2006) where mixing of different fluids containing barium and sulphate, respectively, occurs (Griffith and Paytan, 2012). Moreover, barite and ^{13}C-depleted authigenic carbonate precipitation co-occur at low-temperature hydrothermal springs and/or cold methane/hydrocarbon seeps, where fluids from deeper layers containing methane and Ba^{2+} (leached mainly from K-minerals such as K-feldspar and K-mica) are mixing with seawater near the seafloor (Aloisi et al., 2004; Canet et al., 2003; Hanor, 2000).

The morphology of barite crystals reflects the growth rates and is primarily dependent on the degree of supersaturation (Shikazono 1994). This suggests that the dominant appearance of barite as tabular-bladed, well-developed crystal shapes and only rare dendritic aggregates in Kalana is indicative of slow precipitation rates at a low supersaturation level. Moreover, the barite crystal aggregates in Kalana show higher Sr concentration in central parts/zones of the aggregates and the Sr substitution rate decreases rapidly in the outer parts of the crystals. Jamieson et al. (2016) have shown that in seafloor hydrothermal vent deposits the Sr substitution in barite does not show correlation with crystallization temperature, degrees of mixing between seawater providing sulphate and deep hydrothermal fluid carrying Ba, and fluid Sr concentrations, but is a function of crystal growth rate whereas higher degrees of Sr substitution reflect periods of faster crystal growth driven by a higher degree of supersaturation. The decrease of the Sr concentration in the barite aggregates in Kalana suggests that over time the fluid became progressively less saturated with respect to barite in the Kalana fracture-cave systems. The first stages of barite crystallization were characterized by high growth rates under rapidly oscillating environmental conditions (possibly temperature) indicated by the fine zonation of barite crystal cores, whereas zones grow wider and show lower Sr concentration towards the outer faces of crystals, suggesting lower crystal growth rates under lower supersaturation conditions and possibly more stable environmental conditions.

Additionally, origin of the fluids running in Kalana cave systems can be interpreted using the Sr-isotope composition of barite as far as there is no isotopic fractionation of Sr during barite precipitation (Hanor, 2000). If Sr was derived from seawater or from the dissolution of normal marine carbonate host rocks then barite would have a marine isotopic signature. Sr-isotope ratios in the barite sampled in Kalana, however, vary narrowly from 0.711410 to 0.712033 and are very different of Palaeozoic values of 0.7077–0.7092 (McArthur et al., 2001) or modern seawater with $^{87}Sr/^{86}Sr$ value of 0.709183 (Butterfield et al., 2001). This range of the enrichment of $^{87}Sr/^{86}Sr$ ratios (0.003–0.004) in comparison with seawater values contemporaneous or coeval with the depositional age of the host sediment is typical to Palaeozoic stratiform and specifically to the cratonic hydrothermal barite deposits (Maynard et al., 1995). A similar discrepancy of barite and seawater isotopic compositions has also been observed in modern fluids discharging at cold seeps that have been interpreted to reflect the rock-water interaction of fluids before venting at the seafloor (Naehr et al., 2000; Torres et al., 2003). Therefore, we interpret the enrichment in Sr isotope ratios in Kalana barite to represent the excess radiogenic Sr derived from the alteration of silicates (e.g., K-feldspar) during the passage of the fluids in host rocks. This indicates that the barite in Kalana was not deposited (at least not directly) from seawater, but from evolved/deeper fluids.

Similarly to the Sr-isotope ratios there is a negligible fractionation of sulphate S-isotopes during the crystallization of sulphate minerals (c. 1.65‰). The $\delta^{34}S$ values of barite therefore represent the S-isotope composition of the dissolved sulphate in the barite precipitating fluid (Seal et al., 2000). The $\delta^{34}S$

values of seawater dissolved sulphate in Phanerozoic varied from about 35‰ in Cambrian–Ordovician, started to decline from 35‰ to 21.5‰ in Silurian, dropped further down to about 18–20‰ for the most of Devonian and reached around 12–15‰ in Carboniferous and Permian, finally trending back to about 20–22‰ about 45 million years ago (Algeo et al., 2015; Kampschulte and Strauss, 2004; Paytan et al., 1998). The age of speleothem precipitation in Kalana is not known (Eensaar et al., 2017b – PAPER II), but if the seawater is considered as the reservoir providing sulphate then the large spread of measured $\delta^{34}S$ values from 13 to 33‰ would be seemingly consistent with precipitation over a long time period from late Paleozoic to Cenozoic. Nevertheless, barite formation over such a long time period is highly unlikely and the large variation in barite S-isotope composition can instead be explained by bacterial sulphate reworking in a closed system through a Rayleigh-type fractionation process or in an open system with limited sulphate resupply (Canfield, 2001). Bacterial consumption of sulphate (bacterial sulphate reduction – BSR) causes enrichment of the ^{34}S isotope of the residual sulphate in the fluid and as a result the barite precipitating coevally with the progressing BSR becomes isotopically enriched with respect to the heavy S isotopes. The lowest $\delta^{34}S$ values (c. 13‰) found in the central parts of the barite crystals in Kalana could then be considered to represent the composition of the initial dissolved sulphate while the ^{34}S enrichment during crystal growth shows the evolution of the sulphate pool during the BSR.

Seawater sulphate $\delta^{34}S$ values of comparable range (<15‰) were attained by Carboniferous (c. 330 Ma) and were maintained through Permian (Kampschulte and Strauss, 2004), thus delimiting the age of barite precipitation. It is generally assumed that the Carboniferous–Permian seas did not reach the present day Estonian territory and that the area was emerged from sea since the late Devonian. However, the Carboniferous–Permian marine deposits occur in the erosional surface below the Quaternary glacial sediments in Southwestern Latvia and Lithuania (Paškevicius, 1997). The full extent of the sea during Carboniferous and Permian in the Baltic basin is not known and it could be speculated that the Carboniferous and Permian seas bearing sulphate with low $\delta^{34}S$ values also invaded low-laying coastal areas about 200–300 km north of the area where these deposits have preserved in the present day erosional surface. The long erosional period (<250 million years) since the end of Permian would have effectively eroded away the Carboniferous-Permian deposits if any ever existed in the area under study. Interestingly enough, Liivrand (1990) has described redeposited Carboniferous spores in the Quaternary tills in Southern Estonia and Northern Latvia that would further support this hypothesis. The late Paleozoic age of Kalana speleothem structures and mineralization is further supported by the fact that the carbonate rocks in Kalana bear a late Paleozoic–Triassic overprinting on rock magnetization, possibly driven by continental-scale fluid-flow event. (Preeden et al. 2008).

Alternatively, the sulphate provided for barite crystallization could have originated from (a) direct dissolution of evaporates, (b) oxidation of sulphide

minerals or (c) mineralization of organic matter. There are no evaporite deposits known to exist in the rock sequences of the area where the Kalana cave systems are located. Occurrences of gypsum in the upper Devonian lagoonal evaporitic carbonate-claystone sequences in Latvia and northwestern Russia, right next to Estonia, show $\delta^{34}S$ values of >22‰ and cannot be considered as the source of the sulphate. Sedimentary-diagenetic pyrite is a common accessory mineral in the Silurian carbonate rock sequences in Estonia with the $\delta^{34}S$ values in the lowermost Silurian rocks at about –20‰ (Hints et al., 2014). However, the sulphate produced by abiotic and/or biotic low temperature oxidation of sulphide minerals has $\delta^{34}S$ values of sulphate close to those of the source sulphides (Heidel et al., 2013), which would suggest a much more ^{34}S-depleted composition of the original sulphate compared with that measured in the barites with even the lowest $\delta^{34}S$ values.

On the other hand, the sulphur can be derived from the thermal degradation of organosulfur compounds, which results in H_2S with an isotopic composition that is close (within 1–3‰) to its parent organic matter/kerogen (Amrani et al., 2005). The sulphur isotopic composition of sedimentary organic matter depends on its origin and the maturation/ sulfurization processes (Amrani, 2014). As the result, the $\delta^{34}S$ values in the marine sedimentary organosulphur compounds can vary largely but are typically enriched in ^{34}S by up to 30‰ (in average 10‰) relative to co-existing pyrite (Anderson and Pratt, 1995). Hypothetically, if the H_2S derived from the thermal maturation of this source is quantitatively oxidised into the sulphate through several intermediate species, including elemental sulphur, sulphite and thiosulphate (Zhang and Millero, 1994), then the dissolved sulphate would have an isotopic composition of up to c. 10‰. That is in the range of the lowest barite $\delta^{34}S$ values in Kalana. A similar oxidation process of (magmatically derived) H_2S and barite precipitation has been widely described in hydrothermal systems (Rye, 2005).

5.2.3. Fluid evolution in cave-like systems

Oxygen isotopic values of authigenic calcite (within the range of typical speleothem oxygen isotope values) are controlled under equilibrium conditions by the isotopic composition of the dip water, and the temperature (Lachniet, 2009). The $\delta^{18}O$ values of −4.5 to −11.4‰ in 13C depleted carbonates in Kalana are atypical of authigenic cold-seep carbonates that were precipitated in equilibrium or in near equilibrium with seawater and have $\delta^{18}O$ values between –2 and 8‰ (Campbell, 2006). The oxygen isotope composition of calcite precipitated in equilibrium with Phanerozoic seawater varies within −2.0 to –5.0‰ (Veizer et al., 1999). Authigenic seep carbonates, however, may show also slightly positive $\delta^{18}O$ values (up to 2–3‰ higher than equilibrium values), interpreted as being caused by the dissociation of the locally abundant gas hydrate (Feng et al., 2014). The oxygen isotope composition of Kalana speleothem-like structures suggests therefore that the authigenic calcite was

precipitated from fluids with $\delta^{18}O$ values much different from those of normal marine seawater. It is also particularly interesting that the most negative oxygen isotope composition of Kalana speleothem calcite is coupled with the most negative $\delta^{13}C$ values.

Low oxygen isotopic values can point to either (a) the influence of meteoric water or (b) inflow of high-temperature fluids. Alternatively, low-temperature alteration of volcanic glass has been suggested as a source of ^{18}O-depleted fluids (Hein et al., 1979). Numerous altered volcanoclastic layers (bentonites) are found in the Silurian stratigraphic succession in the Baltic Basin (Kiipli et al., 2010). However, the alteration of volcanic glass would have a significant effect only at low water/rock ratios of <1 (Jacobsen and Kaufman, 1999), which is not probable in an open system such as the caves and open fractures in Kalana.

The average annual $\delta^{18}O_{SMOW}$ value of modern meteoric water and shallow groundwater in Estonia is c. –11.5‰ (Punning et al., 1987). The expected $\delta^{18}O$ value of calcite precipitated from fluid in equilibrium with meteoric water at a temperature of 7 °C, that is at the mean annual temperature in Estonia (Jaagus et al., 2014) would be –8.2‰, which is in the range of the observed $\delta^{18}O$ values of bladed-columnar calcite. However, in this case the laminated botryoidal calcite with $\delta^{18}O$ values higher than –6‰ must have been precipitated at temperatures close to or even below 0 °C (Figure 11), which is not plausible. In contrast, if a

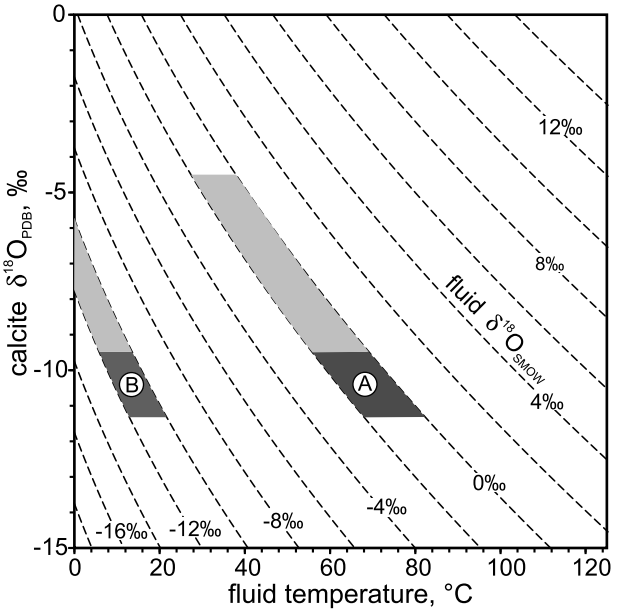

Figure 11. Oxygen isotope fractionation curves for authigenic calcite from the Kalana cave. Dark grey shading represents the spread of δ^{18} O values in columnar-bladed dark calcite, and the light grey area shows variation in δ^{18} O values of laminated botryoidal calcite. Field A illustrates the possible fluid temperatures assuming (sea)water $\delta^{18}O_{SMOW}$ values of –2 to 0 ‰; field B illustrates possible fluid temperatures assuming modern meteoric water ($\delta^{18}O_{SMOW}$ = –12 to –10 ‰) as the fluid source during calcite precipitation. (Eensaar et al., 2017b – PAPER II)

fluid with the oxygen isotopic composition of Phanerozoic seawater –2‰ VSMOW (Veizer et al., 1999) is assumed, the $\delta^{18}O$ values increasing from –11‰ in the central parts of the botryoidal aggregates to –5‰ in their outer parts would indicate the presence of low-temperature hydrothermal fluids, with temperatures decreasing from c. 70 °C during the precipitation of columnar-bladed calcite to about 20 °C during the precipitation of laminated calcite. A similar shift towards lower $\delta^{18}O$ and $\delta^{13}C$ values in altered carbonate bedrock has been reported from caves influenced by thermal waters (Bottrell et al., 2001; Spötl et al., 2009).

Similarly, if the barite was crystallized under equilibrium conditions then the fluid temperatures at the time of barite precipitation can be estimated using the isotope fractionation–temperature equation 2 (Kusakabe and Robinson, 1977). Assuming a fluid with the oxygen isotopic composition of Phanerozoic seawater –2‰ VSMOW (Veizer et al. 1999) the $\delta^{18}O$ values of barite mostly varying between 15–19‰ (median at 17.5‰) would indicate barite precipitation from a

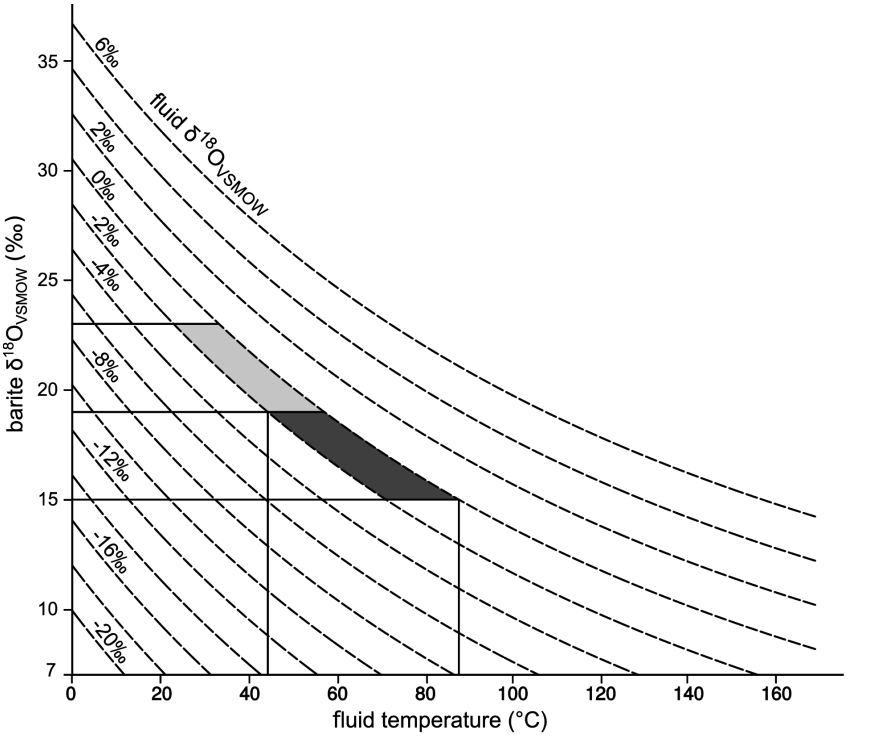

Figure 12. Oxygen isotope fractionation curves for barite from the Kalana cave. Dark grey shading represents the spread of $\delta^{18}O_{SMOW}$ in barite I generation and the light grey area shows variation in $\delta^{18}O_{SMOW}$ values of barite II generation. Shaded areas illustrate the possible fluid temperatures assuming the Phanerozoic (sea)water with $\delta^{18}O_{SMOW}$ values between –2 and 0 ‰ as the fluid source during barite precipitation. (from Gaškov et al., 2017 – PAPER III).

low-temperature hydrothermal fluid, with temperatures of c. 40–70 °C for the I generation of the barite and temperatures of c. 20 °C during the precipitation of the II generation (Figure 12). This range of temperatures agrees well with the fluid temperatures estimated for precipitation of ^{13}C-depleted calcite speleothems crusts succeeding the first barite generation and preceding the second barite generation (Eensaar et al., 2017b – PAPER II). The $\delta^{18}O$ values of these calcite crusts increasing from –11‰ in the central parts of the botryoidal aggregates to –5‰ in the outer parts of the aggregates suggest a cooling of a low temperature hydrothermal fluids from c. 70 °C to ambient.

At the same time there is a trend of increasing Sr-isotope ratios and $\delta^{34}S$ values from the central/core parts of the large barite crystals towards the edges, whereas Sr-isotope ratios and $\delta^{34}S$ values show positive covariation (Figure 13). Such covariation suggests a mixing of two endmember fluids at varying ratios – one being a more evolved fluid with elevated Sr-isotope ratios and isotopically heavy sulphate, possibly derived from reworked porewater, and another being a fluid bearing isotopically light sulphate and less radiogenic Sr-isotope signature, possibly representing the original porewater (Maynard et al., 1995; Valenza et al., 2000). The mixing of two fluids bearing different isotopic signatures instead of a fractionation in a fully closed system is further supported by the range of the measured sulphate $\delta^{18}O$ values. In a closed system the Rayleigh-type fractionation in BSR also enriches the residual sulphate in ^{18}O (Aharon and Fu, 2000). As a result a linear correlation between $\delta^{18}O$ and $\delta^{34}S$ should be established in the residual sulphate pool. However, while the barite in Kalana has large variation of $\delta^{34}S$ values pointing to BSR, then $\delta^{18}O$ values are about 15‰ to 18‰ (in few cases >20‰; Figure 6 in Gaškov et al., 2017 – PAPER III), showing no enrichment in 18O and thus implying that the fractionation

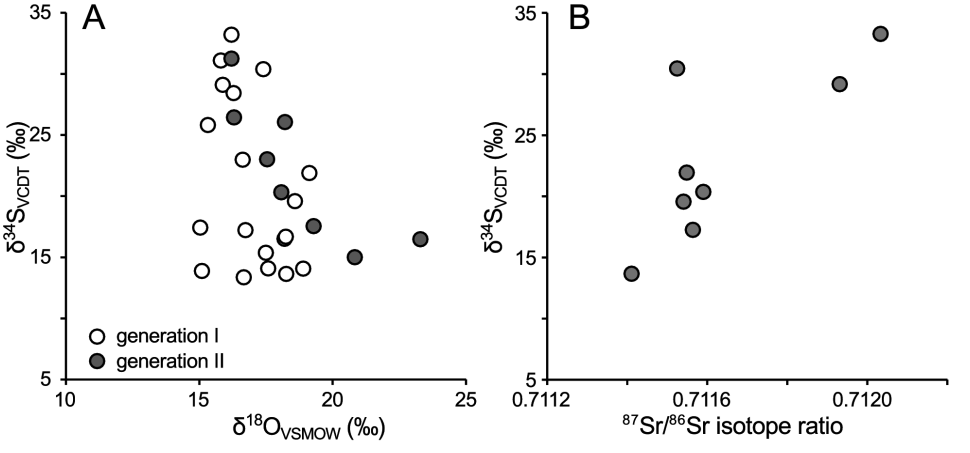

Figure 13. Cross-plot of $\delta^{18}O_{VSMOW}$ and $\delta^{34}S_{VCDT}$ values in barite (A); cross-plot of measured $^{87}Sr/^{86}Sr$ ratios and sulphate $\delta^{34}S_{VCDT}$ values (B). (Gaškov et al., 2017 – PAPER III)

process, if involving bacteria, did not proceed in a closed system, but rather in an open system with (limited) sulphate resupply. In this case the $\delta^{18}O$ values of sulphate are apparently equilibrated with the water composition, meaning that the paired fractionation of sulphur and oxygen during BSR had minimal effect on oxygen isotopic composition.

The formation of ^{13}C-depleted calcitic speleothems and barite-pyrite aggregates in Kalana could be viewed not as a common karstic feature in the vadoze zone of the fractured carbonate strata, but rather as a hypogenic-hydrothermal (karst) system (Klimchouk, 2009; Palmer, 2011; Spötl et al., 2009), developed in the phreatic zone of fracture systems at the mixing front of oxygenated seawater or groundwater and low-temperature reducing methane and Ba-bearing hydrothermal fluids. The phreatic (underwater) environment of calcite precipitation is supported by columnar to fibrous fabrics of authigenic calcite in Kalana caves, which suggests calcite precipitation in continuously wet, low hydrodynamic conditions from a water fluid at low supersaturation with respect to calcite (Frisia et al., 2000). Moreover, Palmer (2011) pointed out that hypogenic caves are typically formed at mixing fronts of two or more waters of contrasting chemistry, e.g. when rising H_2S-rich water encounters oxygen-rich water or at the cooling of rising thermal water carrying aggressive solutions generated by the maturation of hydrocarbons and/or metamorphism of carbonate rocks. In this case the carbon and oxygen isotopic composition of the speleothem calcite and oxygen and strontium isotopic composition of the barite in Kalana reflects the cooling and/or mixing of a warm fluid (possibly up to 70 °C) containing carbon and sulphur derived from anaerobic oxidation of biogenic methane diluted by oxygenated fluids carrying inorganic carbon and or sulphate.

The age of these precipitates in the Kalana cave system cannot be assessed at the present state of knowledge. Still, the hydrothermal signature in the oxygen isotope composition in AOM calcite and barite suggests that its formation could be tentatively tied to either Late Palaeozoic–Triassic low-temperature hydrothermal overprinting on rock magnetization revealed in carbonate rocks in Kalana (Preeden et al., 2008), or to far-field hydrothermal influences of the latest phase of Caledonian orogeny (425–400 Ma), expressed in the Baltic Basin in late Silurian–Devonian K–Ar isotope ages of illite–smectite in K-bentonites (Somelar et al., 2010).

6. CONCLUSIONS

The aim of this thesis was to study the fluid-driven mineralization, mineral assemblage and paragenesis, and fluid characteristics in fracture-controlled cave and vein systems in the Silurian carbonate succession in Kalana, central Estonia. This study shows that mineralization of sphalerite, barite, and ^{13}C-depleted speleothem calcite in Kalana was driven by low-temperature hydrothermal fluids.

Paragenetically the earliest calcite-sphalerite veins are thin (up to 5 cm wide) irregular branching veins characterized by two generations of sphalerite: the first one nucleated at fracture walls and is followed by blocky calcite, and the second and most abundant sphalerite generation is precipitated in the central parts of the calcite-filled veins. The fluid inclusions in the vein filling calcite are in most cases secondary and deformed. The few measured primary two-phase inclusions have minimum homogenization temperatures between 183 and 201 °C and salinities of 2–3.5 wt% NaCleq. However, the primary two-phase liquid-vapour inclusions in the sphalerite suggest a NaCl-$CaCl_2$-H2O fluid composition with the salinities of the fluids ranging from 24.3 to 27.9 wt% $CaCl_2$eq. The homogenization temperatures for the sphalerite two-phase inclusions vary from 64–200 (220) °C. The first sphalerite generation shows homogenization temperatures between 192–200 °C, and the temperatures measured in the second generation crystals cluster at 60–120 °C.

Cave-like structures exploit the pre-existing fracture systems and are filled with botryoidal calcite precipitates and barite-pyrite crystal aggregates. Speleothem-like calcite in Kalana is atypically to speleothem calcite depleted in ^{13}C. The $\delta^{13}C_{PDB}$ values ranged down to −56‰ in a fracture–cave system exposed in the quarry, indicating anaerobic methane oxidation as the carbon source. The $\delta^{18}O_{PDB}$ values of the most ^{13}C-depleted speleothem-like calcite range from −10 to −12‰, hinting at precipitation at elevated temperatures. Systematic variation in $\delta^{13}C_{PDB}$ and $\delta^{18}O_{PDB}$ values in the layered precipitates indicates a change from an initially biogenic methane source to either thermogenic methane or hydrocarbon source in the low-temperature hydrothermal fluid. Calcite speleothems in Kalana possibly developed at the mixing front of sulphate-rich seawater and/or groundwater and low-temperature methane-bearing hydrothermal fluids in the phreatic zone of a hypogenic-hydrothermal (karst) system. The same environment was responsible for abundant barite and pyrite precipitation under variable oxidative–reducing conditions in association with botryoidal calcite aggregates. Isotope composition of barite suggest the one of the fluids was a low-temperature (warm) reducing fluid bearing Ba, characterized by an elevated radiogenic Sr and ^{34}S enriched isotopic signal, and another, possibly a cooler ambient fluid was bearing isotopically lighter dissolved sulphate, and was characterised by lower Sr-isotope ratios. The sulphate was derived either from the oxidized H_2S developed by thermal maturation of buried sedimentary organic matter or from the seawater source.

The gradual increase in $\delta^{34}S$ values towards the outer zones in the barite crystals in Kalana possibly indicates the presence of bacterial sulphate reduction that causes enrichment of the ^{34}S isotope of the residual sulphate in the fluid, whereas the lack of the paired ^{34}S and ^{18}O enrichment, characteristic to bacterial reworking, indicates an open system with limited sulphate resupply where the $\delta^{18}O$ composition of sulphate was equilibrated with a warm ascending hydrothermal fluid.

The mineralization style, fluid characteristics, and the tectonic setting of calcite-sphalerite veins and Pb-Zn mineralization in the northern part of the Baltic palaeobasin are in general similar to Mississippi Valley Type mineralization. The maximum age can be constrained by cross-cutting relationships to the early Middle Devonian (Eifelian), which is somewhat younger than the Pb-Zn mineralization event at the Scandinavian Caledonian front, but coincides with the age of the fluid-driven illitization of K-bentonite beds and Silurian – Devonian (Carboniferous) remagnetization overprint in the northern Baltic palaeobasin.

The formation of ^{13}C-depleted calcitic speleothems and barite-pyrite in Kalana could be viewed not as a common karstic feature in the vadoze zone of the fractured carbonate strata, but rather as a hypogenic-hydrothermal (karst) system, developed in the phreatic zone of fracture systems at the mixing front of oxygenated seawater or groundwater and low-temperature reducing methane and Ba-bearing hydrothermal fluids. Though poorly constrained the tentative age of Kalana speleothem structures and mineralization would be tied to late Paleozoic–Triassic overprinting on rock magnetization, possibly driven by continental-scale fluid-flow event.

REFERENCES

Aharon, P., Fu, B.S., 2000. Microbial sulfate reduction rates and sulfur and oxygen isotope fractionations at oil and gas seeps in deepwater Gulf of Mexico. Geochimica et Cosmochimica Acta, 64(2): 233–246.

Algeo, T.J., Luo, G.M., Song, H.Y., Lyons, T.W., Canfield, D.E., 2015. Reconstruction of secular variation in seawater sulfate concentrations. Biogeosciences, 12(7): 2131–2151.

Alm, E., Sundblad, K., Huhma, H., 2005. Sm–Nd isotope determinations of low-temperature fluorite-calcite-galena mineralization in the margins of the Fennoscandian Shield. Report of activities carried out during 2004., Swedish Nuclear Fuel and Waste Management Co. (SKB), Stockholm.

Aloisi, G. et al., 2004. The effect of dissolved barium on biogeochemical processes at cold seeps. Geochimica et Cosmochimica Acta, 68(8): 1735–1748.

Amrani, A., 2014. Organosulfur compounds: molecular and isotopic evolution from biota to oil and gas. Annual Review of Earth and Planetary Sciences, 42: 733–768.

Amrani, A., Lewan, M.D., Aizenshtat, Z., 2005. Stable sulfur isotope partitioning during simulated petroleum formation as determined by hydrous pyrolysis of Ghareb Limestone, Israel. Geochimica et Cosmochimica Acta, 69(22): 5317–5331.

Anderson, T.F., Pratt, L.M., 1995. Isotopic evidence for the origin of organic sulfur and elemental sulfur in marine sediments. Geochemical Transformations of Sedimentary Sulfur, 612: 378–396.

Bakker, R.J., 2003. Package FLUIDS 1. Computer programs for analysis of fluid inclusion data and for modelling bulk fluid properties. Chemical Geology, 194(1–3): 3–23.

Beal, E.J., House, C.H., Orphan, V.J., 2009. Manganese- and Iron-Dependent Marine Methane Oxidation. Science, 325(5937): 184–187.

Billström, K., Broman, C., Schneider, J., Pratt, W., Skogsmo, G., 2012. Zn-Pb Ores of Mississippi Valley Type in the Lycksele-Storuman District, Northern Sweden: A Possible Rift-Related Cambrian Mineralisation Event. Minerals, 2(3): 169–207.

Bodnar, R.J., 1993. Revised equation and table for determining the freezing point depression of H2O-NaCl solutions. Geochimica et Cosmochimica Acta, 57(3): 683–684.

Boetius, A. et al., 2000. A marine microbial consortium apparently mediating anaerobic oxidation of methane. Nature, 407(6804): 623–626.

Borisenko, A., 1977. Studies of salinity of gas-liquid inclusions in minerals by the cryometric method. Soviet Geology and Geophysics, 18(8): 16–27.

Bottrell, S.H., Crowley, S., Self, C., 2001. Invasion of a karst aquifer by hydrothermal fluids: evidence from stable isotopic compositions of cave mineralization. Geofluids, 1(2): 103–121.

Brangulis, A., 1985. Vendian and Cambrian of Latvia. Zinatne, Riga, 134 pp.

Breecker, D.O. et al., 2012. The sources and sinks of CO2 in caves under mixed woodland and grassland vegetation. Geochimica et Cosmochimica Acta, 96: 230–246.

Butterfield, D.A., Nelson, B.K., Wheat, C.G., Mottl, M.J., Roe, K.K., 2001. Evidence for basaltic Sr in midocean ridge-flank hydrothermal systems and implications for the global oceanic Sr isotope balance. Geochimica et Cosmochimica Acta, 65(22): 4141–4153.

Campbell, K.A., 2006. Hydrocarbon seep and hydrothermal vent paleoenvironments and paleontology: Past developments and future research directions. Palaeogeography Palaeoclimatology Palaeoecology, 232(2–4): 362–407.

Canet, C., Prol-Ledesma, R.M., Melgarejo, J.C., Reyes, A., 2003. Methane-related carbonates formed at submarine hydrothermal springs: a new setting for microbially-derived carbonates? Marine Geology, 199(3–4): 245–261.

Canfield, D.E., 2001. Isotope fractionation by natural populations of sulfate-reducing bacteria. Geochimica et Cosmochimica Acta, 65(7): 1117–1124.

Castellini, D.G., Dickens, G.R., Snyder, G.T., Ruppel, C.D., 2006. Barium cycling in shallow sediment above active mud volcanoes in the Gulf of Mexico. Chemical Geology, 226(1–2): 1–30.

Cerling, T.E., 1984. The Stable Isotopic Composition of Modern Soil Carbonate and Its Relationship to Climate. Earth and Planetary Science Letters, 71(2): 229–240.

Drake, H. et al., 2015. Extreme C-13 depletion of carbonates formed during oxidation of biogenic methane in fractured granite. Nature Communications, 6.

Drake, H., Tullborg, E.L., 2009. Paleohydrogeological events recorded by stable isotopes, fluid inclusions and trace elements in fracture minerals in crystalline rock, Simpevarp area, SE Sweden. Applied Geochemistry, 24(4): 715–732.

Drake, H., Tullborg, E.L., Page, L., 2009. Distinguished multiple events of fracture mineralisation related to far-field orogenic effects in Paleoproterozoic crystalline rocks, Simpevarp area, SE Sweden. Lithos, 110(1–4): 37–49.

Eensaar, J. et al., 2017a. Hydrothermal fracture mineralization in the stable cratonic northern part of the Baltic Paleobasin: sphalerite fluid inclusion evidence. GFF, 139(1): 52–62.

Eensaar, J., Pani, T., Gaškov, M., Sepp, H., Kirsimäe, K., 2017b. Stable isotope composition of hypogenic speleothem calcite in Kalana (Estonia) as a record of microbial methanotrophy and fluid evolution. Geological Magazine, 154(1): 57–67.

Ettwig, K.F. et al., 2010. Nitrite-driven anaerobic methane oxidation by oxygenic bacteria. Nature, 464(7288): 543–+.

Fedorenko, J., Menaker, E., 1977. Lead-zinc mineralization in Latvian territory. In: Afanasjev, B. et al. (Eds.), Lithology and mineral resources of Palaeozoic deposits in Baltics. Institute of Marine Geology and Geophysics, Riga, pp. 74–80.

Feng, D. et al., 2014. Time integrated variation of sources of fluids and seepage dynamics archived in authigenic carbonates from Gulf of Mexico Gas Hydrate Seafloor Observatory. Chemical Geology, 385: 129–139.

Frisia, S., Borsato, A., Fairchild, I.J., McDermott, F., 2000. Calcite fabrics, growth mechanisms, and environments of formation in speleothems from the Italian Alps and southwestern Ireland. Journal of Sedimentary Research, 70(5): 1183–1196.

Frisia, S. et al., 2011. Carbon mass-balance modelling and carbon isotope exchange processes in dynamic caves. Geochimica et Cosmochimica Acta, 75(2): 380–400.

Gaškov, M., Sepp, H., Pani, T., Paiste, P., Kirsimäe, K., 2017. Barite mineralization in Kalana speleothems, Central Estonia: Sr, S and O isotope characterization. Estonian Journal of Earth Sciences, 66(3): 130–141.

Genty, D. et al., 1999. Calculation of past dead carbon proportion and variability by the comparison of AMS(14)C and TIMS U/Th ages on two holocene stalagmites. Radiocarbon, 41(3): 251–270.

Griffith, E.M., Paytan, A., 2012. Barite in the ocean – occurrence, geochemistry and palaeoceanographic applications. Sedimentology, 59(6): 1817–1835.

Hanor, J.S., 2000. Barite-celestine geochemistry and environments of formation. In: Alpers, C.N., Jambor, J.L., Nordstrom, K.D. (Eds.), Sulfate Minerals – Crystallography, Geochemistry and Environmental Significance. Reviews in Mineralogy and Geochemistry. Mineralogical Society of America and Geochemical Society, Washington, DC, pp. 193–275.

Heidel, C., Tichomirowa, M., Junghans, M., 2013. Oxygen and sulfur isotope investigations of the oxidation of sulfide mixtures containing pyrite, galena, and sphalerite. Chemical Geology, 342: 29–43.

Hein, J.R., O'Neil, J.R., Jones, M.G., 1979. Origin of authigenic carbonates in sediment from the deep Bering Sea. Sedimentology, 26: 681–705.

Hendriks, B. et al., 2007a. A fission track data compilation for Fennoscandia. Norwegian Journal of Geology, 87(1–2): 143–155.

Hendriks, B.W.H., Donelick, R.A., O'Sullivan, P.B., Redfield, T.F., 2007b. Evidence for natural, non-thermal annealing of fission tracks in apatite. Geochimica et Cosmochimica Acta, 71(15): A395–A395.

Hendriks, B.W.H., Redfield, T.F., 2005a. Apatite fission track and (U-Th)/He data from Fennoscandia: An example of underestimation of fission track annealing in apatite. Earth and Planetary Science Letters, 236(1–2): 443–458.

Hendriks, B.W.H., Redfield, T.F., 2005b. Evidence for underestimation of long term FT annealing in apatite from natural FT and (U-Th)/He data. Geochimica et Cosmochimica Acta, 69(10): A298–A298.

Himmler, T., Freiwald, A., Stollhofen, H., Peckmann, J., 2008. Late Carboniferous hydrocarbon-seep carbonates from the glaciomarine Dwyka Group, southern Namibia. Palaeogeography Palaeoclimatology Palaeoecology, 257(1–2): 185–197.

Hints, O. et al., 2014. New data on Ordovician stable isotope record and conodont biostratigraphy from the Viki reference drill core, Saaremaa Island, western Estonia. GFF, 136(1): 100–104.

Hints, R., Kirsimäe, K., Somelar, P., Kallaste, T., Kiipli, T., 2008. Multiphase Silurian bentonites in the Baltic Palaeobasin. Sedimentary Geology, 209(1–4): 69–79.

Hints, R., Kirsimäe, K., Somelar, P., Kallaste, T., Kiipli, T., 2006. Chloritization of Late Ordovician K-bentonites from the northern Baltic Palaeobasin-influence from source material or diagenetic environment? Sedimentary Geology, 191(1–2): 55–66.

Högdahl, K., Gromet, L.P., Broman, C., 2001. Low P-T Caledonian resetting of U-rich Paleoproterozoic zircons, central Sweden. American Mineralogist, 86(4): 534–546.

Jaagus, J., Briede, A., Rimkus, E., Remm, K., 2014. Variability and trends in daily minimum and maximum temperatures and in the diurnal temperature range in Lithuania, Latvia and Estonia in 1951–2010. Theoretical and Applied Climatology, 118(1–2): 57–68.

Jacobsen, S.B., Kaufman, A.J., 1999. The Sr, C and O isotopic evolution of Neoproterozoic seawater. Chemical Geology, 161(1–3): 37–57.

Jamieson, J.W. et al., 2016. Precipitation and growth of barite within hydrothermal vent deposits from the Endeavour Segment, Juan de Fuca Ridge. Geochimica et Cosmochimica Acta, 173: 64–85.

Joye, S.B., Bowles, M.W., Samarkin, V.A., Hunter, K.S., Niemann, H., 2010. Biogeochemical signatures and microbial activity of different cold-seep habitats along the Gulf of Mexico deep slope. Deep-Sea Research Part Ii-Topical Studies in Oceanography, 57(21–23): 1990–2001.

Kaljo, D., Martma, T., 2000. Carbon isotopic composition of Llandovery rocks (East Baltic Silurian) with environmental interpretation. Proceedings of the Estonian Academy of Sciences. Geology, 49(4): 267–283.

Kampschulte, A., Strauss, H., 2004. The sulfur isotopic evolution of Phanerozoic seawater based on the analysis of structurally substituted sulfate in carbonates. Chemical Geology, 204(3–4): 255–286.

Katinas, V., Nawrocki, J., 2004. Mesozoic remagnetization of Upper Devonian carbonates from the Cesis and Skaistgirys quarries (Baltic states). Geological Quarterly, 48(3): 293–298.

Kendrick, M.A., Burgess, R., Harrison, D., Bjorlykke, A., 2005. Noble gas and halogen evidence for the origin of Scandinavian sandstone-hosted Pb-Zn deposits. Geochimica et Cosmochimica Acta, 69(1): 109–129.

Khramov, A.N., Iosifidi, A.G., 2009. Paleomagnetism of the Lower Ordovician and Cambrian sedimentary rocks in the section of the Narva River right bank: For the construction of the Baltic Kinematic model in the Early Paleozoic. Izvestiya-Physics of the Solid Earth, 45(6): 465–481.

Kiipli, T., Kallaste, T., Nestor, V., 2010. Composition and correlation of volcanic ash beds of Silurian age from the eastern Baltic. Geological Magazine, 147(6): 895–909.

Kiipli, T. et al., 2007. Altered volcanic ash as an indicator of marine environment, reflecting pH and sedimentation rate – Example from the Ordovician-Kinnekulle bed of Baltoscandia. Clays and Clay Minerals, 55(2): 177–188.

Kirsimäe, K., Jorgensen, P., 2000. Mineralogical and Rb-Sr isotope studies of low-temperature diagenesis of Lower Cambrian clays of the Baltic paleobasin of North Estonia. Clays and Clay Minerals, 48(1): 95–105.

Kirsimäe, K., Kalm, V., Jorgensen, P., 1999. Diagenetic transformation of clay minerals in Lower Cambrian argillaceous sediments of North Estonia. Proceedings of the Estonian Academy of Sciences. Geology, 48: 15–34

Klimchouk, A., 2009. Morphogenesis of hypogenic caves. Geomorphology, 106(1–2): 100–117.

Kukkonen, I.T., Jõeleht, A., 2003. Weichselian temperatures from geothermal heat flow data. Journal of Geophysical Research-Solid Earth, 108(B3).

Kusakabe, M., Robinson, B.W., 1977. Oxygen and sulfur isotope equilibria in the BaSO4-HSO4−-H2O system from 110 to 350°C and applications. Geochimica et Cosmochimica Acta, 41(8): 1033–1040.

Lachniet, M.S., 2009. Climatic and environmental controls on speleothem oxygen-isotope values. Quaternary Science Reviews, 28(5–6): 412–432.

Lazauskienė, J., Marshall, J.E.A., 2002. Chitinozoan reflectance and the thermal history of the Lower Palaeozoic sediments of the Baltic Basin, 5th Baltic Stratigraphic Conference. Vilnius University, Vilnius, pp. 93–97.

Leach, D.L. et al., 2010. Sediment-Hosted Lead-Zinc Deposits in Earth History. Economic Geology, 105(3): 593–625.

Liivrand, E., 1990. Methodical problems of Pleistocene palynostratigraphy. Valgus, Tallinn, 176 pp.

Lindblöm, S., 1986. Textural and fluid inclusion evidence for ore deposition in the Pb-Zn deposit at Laisvall, Sweden. Economic Geology, 81(1): 46–64.

Markovic, S., Paytan, A., Li, H., Wortmann, U.G., 2016. A revised seawater sulfate oxygen isotope record for the last 4 Myr. Geochimica et Cosmochimica Acta, 175: 239–251.

Marlow, J., Peckmann, J., Orphan, V., 2015. Autoendoliths: a distinct type of rock-hosted microbial life. Geobiology, 13(4): 303–307.
Maynard, J.B., Morton, J., Valdes-Nodarse, E.L., Diaz-Carmona, A., 1995. Sr isotopes of bedded barites: Guide to distinguishing basins with Pb-Zn mineralization. Economic Geology and the Bulletin of the Society of Economic Geologists, 90(7): 2058–2064.
McArthur, J.M., Howarth, R.J., Bailey, T.R., 2001. Strontium isotope stratigraphy: LOWESS version 3: Best fit to the marine Sr-isotope curve for 0-509 Ma and accompanying look-up table for deriving numerical age. Journal of Geology, 109(2): 155–170.
McDermott, F., 2004. Palaeo-climate reconstruction from stable isotope variations in speleothems: a review. Quaternary Science Reviews, 23(7–8): 901–918.
Mernagh, T.P., Wilde, A.R., 1989. The Use of the Laser Raman Microprobe for the Determination of Salinity in Fluid Inclusions. Geochimica et Cosmochimica Acta, 53(4): 765–771.
Middleton, M.F., Tullborg, E.L., Larson, S.A., Björklund, L., 1996. Modelling of a Caledonian foreland basin in Sweden: Petrophysical constraints. Marine and Petroleum Geology, 13(4): 407–413.
Milnes, A.G., 1998. Alpine and Caledonide tectonics – a brief comparative study. Gff, 120: 237–247.
Milucka, J. et al., 2012. Zero-valent sulphur is a key intermediate in marine methane oxidation. Nature, 491(7425): 541–+.
Motuza, G., Sliaupa, S., Timmerman, M.J., 2015. Geochemistry and Ar-40/Ar-39 age of Early Carboniferous dolerite sills in the southern Baltic Sea. Estonian Journal of Earth Sciences, 64(3): 233–248.
Murrell, G.R., Andriessen, P.A.M., 2004. Unravelling a long-term multi-event thermal record in the cratonic interior of southern Finland through apatite fission track thermochronology. Physics and Chemistry of the Earth, 29(10): 695–706.
Männik, P., Tinn, O., Loydell, D.K., Ainsaar, L., 2016. Age of the Kalana Lagerstatte, early Silurian, Estonia. Estonian Journal of Earth Sciences, 65(2): 105–114.
Naehr, T.H., Stakes, D.S., Moore, W.S., 2000. Mass wasting, ephemeral fluid flow, and barite deposition on the California continental margin. Geology, 28(4): 315–318.
Natalicchio, M. et al., 2012. Polyphasic carbonate precipitation in the shallow subsurface: Insights from microbially-formed authigenic carbonate beds in upper Miocene sediments of the Tertiary Piedmont Basin (NW Italy). Palaeogeography Palaeoclimatology Palaeoecology, 329: 158–172.
Nestor, H., Einasto, R., 1997. Ordovician and Silurian carbonate sedimentation basin. In: Raukas, A., Teedumäe, A. (Eds.), Geology and Mineral Resources of Estonia. Estonian Academy Publishers, Tallinn, pp. 192–204.
Nikishin, A.M. et al., 1996. Late Precambrian to Triassic history of the East European Craton: Dynamics of sedimentary basin evolution. Tectonophysics, 268(1–4): 23–63.
O'Neil, J.R., Clayton, R.N., Mayeda, T.K., 1969. Oxygen Isotope Fractionation in Divalent Metal Carbonates. The Journal of Chemical Physics, 51(12): 5547–5558.
Oakes, C.S., Bodnar, R.J., Simonson, J.M., 1990. The System Nacl-Cacl2-H2o .1. The Ice Liquidus at 1 Atm Total Pressure. Geochimica et Cosmochimica Acta, 54(3): 603–610.
Orphan, V.J., House, C.H., Hinrichs, K.U., McKeegan, K.D., DeLong, E.F., 2002. Multiple archaeal groups mediate methane oxidation in anoxic cold seep sediments.

Proceedings of the National Academy of Sciences of the United States of America, 99(11): 7663–7668.
Palmer, A.N., 2011. Distinction between epigenic and hypogenic maze caves. Geomorphology, 134(1–2): 9–22.
Palmre, H., 1967. Texture of lead-zinc ore occurrences in Estonia. Proceedings of the Academy of Sciences of the Estonian SSR. Chemistry. Geology, 16(3): 229–237.
Paškevicius, J., 1997. The geology of the Baltic Republics. Lietuvos geologijos tarnyba, Vilnius, 387 pp.
Paull, C.K. et al., 1992. Indicators of methane-derived carbonates and chemosynthetic organic carbon deposits; examples from the Florida Escarpment. Palaios, 7(4): 361–375.
Paytan, A., Kastner, M., Campbell, D., Thiemens, M.H., 1998. Sulfur isotopic composition of Cenozoic seawater sulfate. Science, 282(5393): 1459–1462.
Peckmann, J., Paul, J., Thiel, V., 1999. Bacterially mediated formation of diagenetic aragonite and native sulfur in Zechstein carbonates (Upper Permian, Central Germany). Sedimentary Geology, 126(1–4): 205–222.
Peckmann, J., Thiel, V., 2004. Carbon cycling at ancient methane-seeps. Chemical Geology, 205(3–4): 443–467.
Pedersen, K., 2013. Metabolic activity of subterranean microbial communities in deep granitic groundwater supplemented with methane and H-2. Isme Journal, 7(4): 839–849.
Pichugin, M.S., Puura, V., Vingisaar, P., Erisalu, E., 1976. Regional metasomatic dolomitization associated with tectonic disturbances in Lower Paleozoic deposits of the northern Baltic region. Soviet Geology, 10: 78–90.
Pin, C., Bassin, C., 1992. Evaluation of a strontium-specific extraction chromatographic method for isotopic analysis in geological-materials. Analytica Chimica Acta, 269(2): 249–255.
Plado, J., Preeden, U., Pesonen, L.J., Mertanen, S., Puura, V., 2010. Magnetic history of Early and Middle Ordovician sedimentary sequence, northern Estonia. Geophysical Journal International, 180(1): 147–157.
Plado, J. et al., 2008. Palaeomagnetic age of remagnetizations in Silurian dolomites, Rõstla quarry (Central Estonia). Geological Quarterly, 52(3): 213–224.
Plink-Björklund, P., Björklund, L., 1999. Sedimentary response in the Baltic Devonian Basin to post-collisional events in the Scandinavian Caledonides. GFF, 121(1): 79–80.
Poprawa, P., Šliaupa, S., Stephenson, R., Lazauskiene, J., 1999. Late Vendian-Early Palaeozoic tectonic evolution of the Baltic Basin: regional tectonic implications from subsidence analysis. Tectonophysics, 314(1–3): 219–239.
Preeden, U., Mertanen, S., Elminen, T., Plado, J., 2009. Secondary magnetizations in shear and fault zones in southern Finland. Tectonophysics, 479(3–4): 203–213.
Preeden, U., Plado, J., Mertanen, S., Puura, V., 2008. Multiply remagnetized Silurian carbonate sequence in Estonia. Estonian Journal of Earth Sciences, 57(3): 170–180.
Punning, J.M., Vaikmäe, R., Tõugu, K., 1987. Variations of Delta-18o and Cl- in the Ice Cores of Spitsbergen. Journal De Physique, 48(C–1): 619–624.
Puura, V., Vaher, R., 1997. Cover structure. In: Raukas, A., Teedumäe, A. (Eds.), Geology and mineral resources of Estonia. Estonian Academy Publishers, Tallinn, pp. 167–177.

Raidla, V. et al., 2014. Sulphur isotope composition of dissolved sulphate in the Cambrian-Vendian aquifer system in the northern part of the Baltic Artesian Basin. Chemical Geology, 383: 147–154.

Raudsep, R., 1997. Mineral occurrences. In: Raukas, A., Teedumäe, A. (Eds.), Geology and mineral resources of Estonia. Estonian Academy Publishers, Tallinn, pp. 396–372.

Rickard, D.T., Lindblom, S., 1979. Fluid inclusion and related studies of sphalerite from the Laisvall sandstone lead-zinc deposit, Sweden. Annales de la Societe Geologique de Belgique, 102: 485–495.

Rickard, D.T., Willden, M.Y., Marinder, N.E., Donnelly, T.H., 1979. Studies on the genesis of the Laisvall sandstone lead-zinc deposit, Sweden. Economic Geology, 74(5): 1255–1285.

Roberts, H.H., Feng, D., Joye, S.B., 2010. Cold-seep carbonates of the middle and lower continental slope, northern Gulf of Mexico. Deep-Sea Research Part Ii-Topical Studies in Oceanography, 57(21–23): 2040–2054.

Roedder, E., 1984. Fluid inclusions. Reviews in Mineralogy, 12. Mineralogical Society of America, 646 pp.

Romanek, C.S., Grossman, E.L., Morse, J.W., 1992. Carbon Isotopic Fractionation in Synthetic Aragonite and Calcite – Effects of Temperature and Precipitation Rate. Geochimica et Cosmochimica Acta, 56(1): 419–430.

Rye, R.O., 2005. A review of the stable-isotope geochemistry of sulfate minerals in selected igneous environments and related hydrothermal systems. Chemical Geology, 215(1–4): 5–36.

Sahlstedt, E., Karhu, J.A., Pitkanen, P., 2010. Indications for the past redox environments in deep groundwaters from the isotopic composition of carbon and oxygen in fracture calcite, Olkiluoto, SW Finland. Isotopes in Environmental and Health Studies, 46(3): 370–391.

Sahlstedt, E., Karhu, J.A., Pitkanen, P., Whitehouse, M., 2013. Implications of sulfur isotope fractionation in fracture-filling sulfides in crystalline bedrock, Olkiluoto, Finland. Applied Geochemistry, 32: 52–69.

Saintilan, N.J. et al., 2015. A Middle Ordovician Age for the Laisvall Sandstone-Hosted Pb-Zn Deposit, Sweden: A Response to Early Caledonian Orogenic Activity. Economic Geology, 110(7): 1779–1801.

Sandström, B., Tullborg, E.L., 2009. Episodic fluid migration in the Fennoscandian Shield recorded by stable isotopes, rare earth elements and fluid inclusions in fracture minerals at Forsmark, Sweden. Chemical Geology, 266(3–4): 126–142.

Sandström, B., Tullborg, E.L., De Torres, T., Ortiz, J.E., 2006. The occurrence and potential origin of asphaltite in bedrock fractures, Forsmark, central Sweden. Gff, 128: 233–242.

Sandström, B., Tullborg, E.L., Larson, S.A., Page, L., 2009. Brittle tectonothermal evolution in the Forsmark area, central Fennoscandian Shield, recorded by paragenesis, orientation and Ar-40/Ar-39 geochronology of fracture minerals. Tectonophysics, 478(3–4): 158–174.

Sapart, C.J. et al., 2012. Natural and anthropogenic variations in methane sources during the past two millennia. Nature, 490(7418): 85–88.

Schoell, M., 1988. Multiple Origins of Methane in the Earth. Chemical Geology, 71(1–3): 1–10.

Seal, R.R., Alpers, C.N., Rye, R.O., 2000. Stable isotope systematics of sulfate minerals. Sulfate Minerals – Crystallography, Geochemistry and Environmental Significance, 40: 541–602.

Sherlock, S.C., Lucks, T., Kelley, S.P., Barnicoat, A., 2005. A high resolution record of multiple diagenetic events: Ultraviolet laser microprobe Ar/Ar analysis of zoned K-feldspar overgrowths. Earth and Planetary Science Letters, 238(3–4): 329–341.

Smethurst, M.A., Khramov, A.N., Pisarevsky, S., 1998. Palaeomagnetism of the Lower Ordovician Orthoceras Limestone, St. Petersburg, and a revised drift history for Baltica in the early Palaeozoic. Geophysical Journal International, 133(1): 44–56.

Somelar, P., Kirsimäe, K., Hints, R., Kirs, J., 2010. Illitization of Early Paleozoic K-Bentonites in the Baltic Basin: Decoupling of Burial- and Fluid-Driven Processes. Clays and Clay Minerals, 58(3): 388–398.

Somelar, P., Kirsimäe, K., Srodon, J., 2009. Mixed-layer illite-smectite in the Kinnekulle K-bentonite, northern Baltic Basin. Clay Minerals, 44(4): 455–468.

Spötl, C., Dublyansky, Y., Meyer, M., Mangini, A., 2009. Identifying low-temperature hydrothermal karst and palaeowaters using stable isotopes: a case study from an alpine cave, Entrische Kirche, Austria. International Journal of Earth Sciences, 98(3): 665–676.

Steiger, R.H., Jäger, E., 1977. Subcommission on geochronology: convention on the use of decay constants in geo- and cosmochronology. Earth and Planetary Science Letters, 36(3): 359–362.

Sundblad, K., Kivisilla, J., Puura, V., Jonsson, E., Fedorenko, J., 1999. Palaeozoic Pb(±Zn) mineralization in the Baltic Sea region. GFF, 121(1): 76–77.

Suuroja, K., 2002. Natural resources of the Kärdla impact structure, Hiiumaa Island, Estonia. In: Plado, J., Pesonen, L.J. (Eds.), Impacts in Precambrian Shields. Impact Studies. Springer, Berlin, pp. 295–306.

Šliaupa, S., Hoth, P., 2011. Geological Evolution and Resources of the Baltic Sea Area from the Precambrian to the Quaternary. In: Harff, J., Björck, S., Hoth, P. (Eds.), The Baltic Sea Basin. Springer Berlin Heidelberg, Berlin, Heidelberg, pp. 13–51.

Šliaupa, S., Poprawa, P., Jacyna, J., 2000. Structural analysis of seismic data in the Baltic Basin: evidences for Silurian–Early Devonian intra-plate compression in the foreland of Caledonian orogen. Journal of Czech Geological Society, 45: 260–261.

Zdanavičiūtė, O., Swadowska, E., 2002. Petrographic and pyrolysis-gas chromatography investigations of the Lower Palaeozoic organic matter of Lithuania. Geologija, 40: 15–23.

Zhang, J.Z., Millero, F.J., 1994. Kinetics of oxidation of hydrogen-sulfide in natural-waters. Environmental Geochemistry of Sulfide Oxidation, 550: 393–409.

Zheng, Y.F., Hoefs, J., 1993. Carbon and Oxygen Isotopic Covariations in Hydro-thermal Calcites – Theoretical Modeling on Mixing Processes and Application to Pb-Zn Deposits in the Harz Mountains, Germany. Mineralium Deposita, 28(2): 79–89.

Ziegler, P.A., 1987. Evolution of the Arctic – North Atlantic borderlands. In: Brooks, J., Glennie, K.W. (Eds.), Petroleum Geology of North West Europe. Graham and Trotman, London, pp. 1201–1204.

Talyzina, N.M., 1998. Fluorescence intensity in Early Cambrian acritarchs from Estonia. Review of Palaeobotany and Palynology, 100(1–2): 99–108.

Talyzina, N.M., Moldowan, J.M., Johannisson, A., Fago, F.J., 2000. Affinities of Early Cambrian acritarchs studied by using microscopy, fluorescence flow cytometry and biomarkers. Review of Palaeobotany and Palynology, 108(1–2): 37–53.

Taylor, J.C., 1991. Computer programs for standardless quantitative analysis of minerals using the full powder diffraction profile. Powder Diffraction, 6: 2–9.
Tinn, O., Meidla, T., Ainsaar, L., Pani, T., 2009. Thallophytic algal flora from a new Silurian Lagerstätte. Estonian Journal of Earth Sciences, 58(1): 38–42.
Tissot, B.P., Welte, D.H., 1984. Petroleum formation and occurrence. Springer-Verlag, New York, 699 pp.
Torres, M.E., Bohrmann, G., Dube, T.E., Poole, F.G., 2003. Formation of modern and Paleozoic stratiform barite at cold methane seeps on continental margins. Geology, 31(10): 897–900.
Torsvik, T.H., Rehnström, E.F., 2003. The Tornquist Sea and Baltica-Avalonia docking. Tectonophysics, 362(1–4): 67–82.
Usaityte, D., 2000. The geology of the southeastern Baltic Sea: a review. Earth-Science Reviews, 50(3–4): 137–225.
Valenza, K., Moritz, R., Mouttaqi, A., Fontignie, D., Sharp, Z., 2000. Vein and karst barite deposits in the western Jebilet of Morocco: Fluid inclusion and isotope (S, O, Sr) evidence for regional fluid mixing related to central Atlantic rifting. Economic Geology and the Bulletin of the Society of Economic Geologists, 95(3): 587–605.
Veizer, J. et al., 1999. 87Sr/86Sr, $\delta^{13}C$ and $\delta^{18}O$ evolution of Phanerozoic seawater. Chemical Geology, 161(1–3): 59–88.
Whiticar, M.J., 1999. Carbon and hydrogen isotope systematics of bacterial formation and oxidation of methane. Chemical Geology, 161(1–3): 291–314.
Yoshinaga, M.Y. et al., 2014. Carbon isotope equilibration during sulphate-limited anaerobic oxidation of methane. Nature Geoscience, 7(3): 190–194.

SUMMARY IN ESTONIAN

Fluidisündmused Balti paleobasseini geoloogilises ajaloos: stabiilsete isotoopide koostis ja fluidisuletiste mikrotermomeetria Siluri karbonaatkivimite läbilõikes, Kalana, Eesti

Maakoores liikuvad (kuumad) lahused ehk fluidid on olulisel kohal Maa geoloogilises ja bioloogilises evolutsioonis. Paljud meile tuntud geoloogilised nähtused on ajendatud fluidide liikumisest või oluliselt mõjutatud fluidide iseloomust.

Balti palebasseini arengut Fanerosoikumis vaadeldakse tüüpiliselt tektooniliselt stabiilse süsteemina, mis on säilitanud oma algse (settimisjärgse) oleku. Samas on selle settekompleksi diageneetilis-mineraalne seisund oluliselt arenenum kui võiks eeldada stabiilsest tektoonilisest režiimist. Lõhelisus ja sellega seostuv dolomiidistumine, samuti üle-eelmisest sajandist tuntud ja eelmise sajandi keskpaigast järgnevatel kümnenditel põhjalikult uuritud polümetalse maagistumise ilmingud ning viimastel kümnenditel enam tähelepanu köitnud kivimite diageneetiliste gradientide uuringud näitavad siiski märkimisväärset fluidilist mõjutust, mis on iseäranis selge ja järsk rikkevööndites, aga esineb ka laiemalt kogu kivimikompleksis. Kivimite diageneetilised gradiendid (iseäranis rikkevööndites) on sageli väga järsud ning enamatel juhtudel ei ole nende häiringute tekkepõhjused selged. Varasemad Balti Basseini Ordoviitsiumi settekivimite ja Fennoskandia kilbi kristalsete kivimite lõhelisustsoonide paleomagnetismiuuringud (nt. Preeden et al., 2009) näitavad valdavalt sekundaarset magnetiseeritust, mille tekkepõhjuseks võib oletada mäestikutekkeliste fluidide levikut orogeneetiliste perioodidega. Fluidisündmustele viitavad ka K-bentoniitide kvaasistabiilse savimineraalide koosluste struktuur ja isotoopvanused (nt. Somelar et al., 2009).

Ajaloolises plaanis ulatuvad hüdrotermaalsete mineralisatsioonide uuringud Eestis 19. sajandisse. Tõsisemalt uuriti sulfiidse mineralisatsiooni ilmingute levikut Eestis (sh Kesk-Eestis Võhma piirkonnas) 20. sajandi teises pooles (nt. Palmre et al., 1967). Suurem osa nendest ilmingutest on tõlgendatud hüdrotermaalseteks, kuigi enamatel juhtudel ei ole nende häiringute tekkepõhjused, fluidide päritolu, koostis ega ka nende laiem geodünaamiline kontekst selge.

Käesoleva doktoritöö eesmärgiks oli uurida fluidide põhjustatud mineralisatsiooni ja fluidide iseloomu Balti paleobasseinis. Fluidide omaduste ja kujunemisloo uuringud keskendusid hüdrotermaalse mineralisatsiooni fluidisuletiste, mineraalide ja karbonaatse-sulfaatse mineralisatsiooni parageneesi uuringutele Kesk-Eesti Siluri karbonaatkivimite läbilõikes, mis on avatud Kalanas (Otisaare karjäär).

Kalana mineralisatsiooni lõhesüsteeme täitvate kaltsiidi-dolomiidi, barüüdi ja sfaleriidi fluidisuletiste mikrotermomeetria näitab, et kaltsiit-sfaleriidi soonte sfaleriidi kristallide primaarsete suletiste sulgumistemperatuurides eristub 3 erineva tekketemperatuuriga sfaleriidi gruppi. Esimene, kõige arvukam rühm on sulgumistemperatuuriga 60–85 °C (keskmine 70 °C), teise rühma homogeniseerumise-sulgumise temperatuur on 95–120 °C ja kolmas, kõige vähemarvukam on rühm, mille sulgumistemperatuur on 190–200 °C. Samas kui soonte kaltsiidi

primaarsete suletiste homogeniseerumise temperatuurid varieeruvad normaaljaotuslikult 115–247 °C vahel. Sfaleriidi suletiste fluidi mikrotermomeetria esimene sulamine (Tfm) toimub –64,3 ºC juures, mis näitab valdavalt $CaCl_2$ koostist. Keskmine Tm sfaleriidis on ~ –34,3 ºC, mis näitab fluidi väga kõrget soolsust, keskmiselt 26,3%.

Paralleelselt mikrotermomeetriliste uuringutega läbiviidud parageneesi uuringud Kalanas lõhesüsteemides näitasid, et sfaleriidi mineralisatsioon paikneb kaltsiit-sfaleriitsetes soontes kahes positsioonis, mida võib tõlgendada sfaleriidi tekkimisena vähemalt kahes etapis. Soonte mineraliseerumise alguses on tekkinud peenekristalliline sfaleriit soonte seintele või on tunginud (asendub) ümbriskivimisse. Seejärel on toimunud kaltsiidi kasvamine, mis on täitnud suurema osa lõhest, kuid lõhede laiematesse osadesse on jäänud vaba ruum. Mineralisatsiooni viimases faasis on toimunud sfaleriidi kasvamine kaltsiidi soonte keskosas ja sfaleriidi agregaadid on täitnud lõhede laiendites olnud tühja ruumi.

Suuremas geodünaamilisemas kontekstis seostub vaadeldud mineralisatsioon Baltica ja Laurentia kokkupõrkega Siluri-Devoni vahetusel ja Kaledoonia pealenihete moodustumisega. Selle loode-kagu suunalises surveväljas tekkinud edela-kirdesuunalised, tavaliselt <50 m vertikaalnihkega murrangud(-vööndid) lõid võimaluse sügavate, kõrge soolsusega fluidide migratsiooniks. Kaledoonia aheliku esine Kesk-Rootsis on tuntud Pb-Zn maagistumise piirkond. Balti paleobasseini polümetalseid maagistumisilminguid võiks selles kontekstis vaadelda kui kagusuunalist Kaledoonia mineralisatsioonivälja pikendust. Siiski, Kaledoonia mineralisatsioon Kesk-Rootsis on valdavalt vanusega 430–400 Ma, samas kui nii Eestis kui ka Lätis on maagistumisilmingute maksimaalne (struktuurne) vanus Kesk-Devonis (390–380 Ma), mida toetavad ka Balti paleobasseini bentoniitide illitiseerumise K-Ar vanused. Üsna silmatorkav on asjaolu, et kuigi tuntud mineralisatsiooni ilmingud Balti paleobasseinis on väga piiratud levikuga, siis erinevalt Skandinaavia Pb-Zn maagistumisest on nende nii fluide koostis kui ka omadused, mineralisatsiooni iseloom ja tektooniline positsioon sarnane nn Mississippi Valley Type (MVT) maagistumisele kogu maailmas.

Olemuslikult vastab selline mineralisatsioon paleomagnetisimi uuringutest (Plado et al. 2008, 2010; Preeden et al. 2008, 2009) tuntud Paleosoikumi fluidisündmusega, mille signaali Siluri kivimites kannab magemiidi magnetiseerituse komponent, mis viitab Hilis-Devoni– Karboni (Mississippi) eale. Samuti näitas Somelar et al. (2009, 2010), et Balti paleobasseinis on Ordoviitsiumi bentoniitide K-Ar meetodil määratud diageneetiline-hüdrotermaalne vanus 370–416 miljonit aastat. See langeb kokku Skandinaavia Kaledoniidide mäestikutekke lõppfaasiga ning orogeneesi poolt põhjustatud madalatemperatuuriliste hüdrotermide liikumisega.

Teine võimalik fluidisündmus, mis ilmneb jääkmagnetismi signaalis ja jääb vanuselist Karbon–Permi piiresse, ei avaldu hüdrotermaalse mineralisatsiooni pildis, oli tõenäoliselt madalatemperatuuriline (<50 °C), hapnikuline ning piiratud reaktiivuse/soolusega, ning arenes eeldatavasti süvapäritolu madalatemperatuurilise hüdrotermaalse fluidi ja pinna(põhja-)vete segunemistsoonis. Selle fluidisündmusega võib seostada unikaalse hüpogeense paleokarsti mine-

ralisatsiooni arengut Kalana läbilõikes. Kõrvuti on kaltsiit-sfaleriit lõhelise mineralisatsiooniga esinevad Kalanas avatud Siluri kivimite läbilõikes koopalised struktuurid, mis on arvatavasti arenenud laienenud lõhedest ja mis on täitunud komplekssе kaltsiidi-püriidi-barüüdi mineralisatsiooniga. Koobaste seintel on kujunenud koorikulised, mitmekihilised kaltsiidi agregaadid, mis meenutavad morfoloogiliselt nn botrüoidseid(keralisi) koopasetted (speleoteeme). Tüüpiliselt on nende mitmekihiliste speoleoteemide paksused kuni mõni cm, kuid võivad ulatuda 10 cm-ni. Kaltsiitsete koorikute tekkimine on toimunud vaheldumisi üksteist asendava püriidi ja barüüdi kristallisatsiooniga. Erinevalt tüüpilistest speleoteemidest iseloomustab kaltsiidi stabiilse isotoopide koostist Kalana koopakoorikutes ekstremaalne vaesustumine ^{13}C suhtes ja $\delta^{13}C_{PDB}$ suur varieeruvus –11‰ kuni –56‰, samas kui δ^{18O}_{PDB} väärtused varieeruvad –5 ‰ kuni −12‰. Niivõrd vaesustunud süsiniku isotoopne koostis viitab selle metanogeensele päritolule. Arvatavasti on nendes koobastes toimunud metaani anaeroobne mikrobiaalne oksüdatsioon ning selle käigus tekkinud vesinikkarbonaadi üleküllastumisel kaltsiidi väljasettimine. Isotoopkoostise ($\delta^{13}C_{PDB}$ ja δ^{18O}_{PDB}) süstemaatiline varieerumine kaltsiitsetes koorikutes nende keskosast väljapoole viitab süsiniku allika muutumisele algselt biogeensest rohkem termogeenseks metaanist või biogeensest metaanist tekkinud vesinikkarbonaadi ja nt mereveest pärineva süsiniku segunemisele. Hapniku isotoopne koostis viitab, et kaltsiidi kristalliseerumine toimus madalatemperatuurilises hüdrotermaalses fluidis (<70 °C) ning tegemist oli nn hüpogeense karstumisega. Seejuures on oluline, et sellist metaani anaeroobse bakteriaalse oksüdatsiooni arvelt tekkinud kaltsiitseid speleoteeme ei ole meile teadaolevalt varem kirjeldatud.

Püriidi ja barüüdi vaheldumine koos speleoteemi kaltsiidiga viitab väljasettimisele sügava-sooja ja Ba-rikka ning sulfaatase mere või põhjavee segunemisfrondil. Seejuures näitavad barüüdi mineralisatsiooni Sr-isotoopide analüüsid, et need hüdrotermaalsed fluidid pärinesid peamiselt üleskuumutatud kontinentaalsetest meteoorsetest vetest ja mitte magmalistest allikatest. Samas viitab süsiniku stabiilsete isotoopide tugev fraktsioneerumine lõhesüsteemidega assotsieerunud kaltsiidis süsiniku metaani päritolule, millega kaasneb sulfaatse väävli bakteriaalne redutseerumine, millest omakorda annab tunnistust tugevalt fraktsioneerunud väävli-isotoopide koostis.

Ka barüüdi ning püriidi teket speleoteemides ja lõhedes saab seletada oksüdeeriva ja redutseeriva keskkonna vaheldumisega. Barüüdi isotoopkoostise alusel võib arvata, et üks fluididest oli hüdrotermaalne (kuni 70 °C) redutseeriv baariumi sisaldav lahus, mida iseloomustab kõrgem radiogeense Sr ning ^{34}S sisaldus, teine aga madalatemperatuuriline kergema isotoopkoostisega lahustunud sulfaati sisaldav fluid. Sulfaatioon pärineb kas mereveest või mattunud orgaanilises aine lagunemisel tekkiva H_2S oksüdeerimisest. ^{34}S sisalduse järkjärguline kasv ühe barüüdi kristalli piires seest väljapoole liikudes viitab fluidis lahustunud sulfaadi bakteriaalsele redutseerimisele. Samas ei ole toimunud barüüdi sulfaadi rikastumist ^{18}O suhtes, mistõttu võib arvata, et tegemist oli süsteemiga, kus sulfaadi $\delta^{18}O$ väärtus tasakaalustus soojade tõusvate hüdotermaalsete fluidide koostisega.

ACKNOWLEDGEMENTS

I am grateful to all my friends and colleagues. Special thanks to Kairi and Pihla.

PUBLICATIONS

CURRICULUM VITAE

Name: Mikk Gaškov
Date of birth: 03.08.1984
Address: Department of Geology, University of Tartu, Ravila 14a, 50411 Tartu, Estonia
Contact: mikk.gaskov@ut.ee

Education

20112017	University of Tartu, Department of Geology PhD student in Geology
2006–2011	University of Tartu, MSc in Geology
2002–2006	University of Tartu, BSc in Geology
1999–2002	Nõo Reaalgmnaasium

Professional employment

2012– 2014	Data analysis specialist, University of Tartu, Department of Geology

Field of research:

geochemistry, geophysics, mineralogy

Publications

Gaškov, M., Sepp, H., Pani, T., Paiste, P., Kirsimäe, K. 2017. Barite mineralization in Kalana speleothems, Central Estonia: Sr, S and O isotope characterization. Estonian Journal of Earth Sciences, 66(3): 130–141.

Eensaar, J., Gaškov, M., Pani, T., Sepp, H., Somelar, P., Kirsimäe, K. 2017a. Hydrothermal fracture mineralization in the stable cratonic northern part of the Baltic Paleobasin: sphalerite fluid inclusion evidence. GFF, 139(1), 52–62.

Eensaar, J., Pani, T., Gaškov, M., Sepp, H. and Kirsimäe, K. 2017b. Stable isotope composition of hypogenic speleothem calcite in Kalana (Estonia) as a record of microbial methanotrophy and fluid evolution. Geological Magazine, 154(1), 57–67.

Gaškov, M., Jõeleht, A. 2012. Soojuspuuraukude mõju põhjaveele. Taastuvate energiallikate uurimine ja kasutamine XIV; Tartu; 8. november 2012. Eds. Normak, A., Suitso, I., Jõgi, E., Vollmer, E., 49−57.

Jõeleht, A., Plado, J., Tuuling, I., Gaškov, M., Rooni, K., Tsyroulnikov, A. 2007. Rim Morphology of the Kärdla Crater Based on Reflection Seismic Investigations. Lunar and Planetary Science XXXVIII, LPI Contribution No. 1338: 38th Lunar and Planetary Science Conference; League City, Texas, USA; March 12–16, 2007. 1615.

Jõeleht, A., Plado, J., Tuuling, I., Gaškov, M., Rooni, K., Tsyrulnikov, A. 2007. Structural features of the Kärdla impact crater's rim as revealed by reflection seismic profiles. Marine impact craters on Earth: Field investigation of the Wetumpka impact structure, a well-preserved marine impact crater, and the K-T boundary in the Alabama Gulf Coastal Plain; Wetumpka, Alabama; Wetumpka Field Forum 2007 Guidebook and Abstracts. Eds. King, D.T., Jr. and Ormö, J. 94−95.

ELULOOKIRJELDUS

Nimi: Mikk Gaškov
Sünniaeg: 03.08.1984
Aadress: Geoloogia osakond, Tartu Ülikool,
Ravila 14a, 50411 Tartu, Eesti
Kontakt: mikk.gaskov@ut.ee

Haridus

2011–2017	Tartu Ülikool, Geoloogia osakond, Geoloogia doktorant
2006–2011	Tartu Ülikool, MSc geoloogias
2002–2006	Tartu Ülikool, BSc geoloogias
1999–2002	Nõo Reaalgümnaasium

Teenistuskäik

2012– 2014	Andmetöötlus spetsialist, Tartu Ülikool, Geoloogia osakond

Teadustöö põhisuunad:

geokeemia, geofüüsika, mineraloogia

Publikatsioonid

Gaškov, M., Sepp, H., Pani, T., Paiste, P., Kirsimäe, K. 2017. Barite mineralization in Kalana speleothems, Central Estonia: Sr, S and O isotope characterization. Estonian Journal of Earth Sciences, 66(3): 130–141.

Eensaar, J., Gaškov, M., Pani, T., Sepp, H., Somelar, P., Kirsimäe, K. 2017a. Hydrothermal fracture mineralization in the stable cratonic northern part of the Baltic Paleobasin: sphalerite fluid inclusion evidence. GFF, 139(1), 52–62.

Eensaar, J., Pani, T., Gaškov, M., Sepp, H. and Kirsimäe, K. 2017b. Stable isotope composition of hypogenic speleothem calcite in Kalana (Estonia) as a record of microbial methanotrophy and fluid evolution. Geological Magazine, 154(1), 57–67.

Gaškov, M., Jõeleht, A. 2012. Soojuspuuraukude mõju põhjaveele. Taastuvate energiallikate uurimine ja kasutamine XIV; Tartu; 8. november 2012. Eds. Normak, A., Suitso, I., Jõgi, E., Vollmer, E., 49−57.

Jõeleht, A., Plado, J., Tuuling, I., Gaškov, M., Rooni, K., Tsyroulnikov, A. 2007. Rim Morphology of the Kärdla Crater Based on Reflection Seismic Investigations. Lunar and Planetary Science XXXVIII, LPI Contribution No. 1338: 38th Lunar and Planetary Science Conference; League City, Texas, USA; March 12–16, 2007. 1615.

Jõeleht, A., Plado, J., Tuuling, I., Gaškov, M., Rooni, K., Tsyrulnikov, A. 2007. Structural features of the Kärdla impact crater's rim as revealed by reflection seismic profiles. Marine impact craters on Earth: Field investigation of the Wetumpka impact structure, a well-preserved marine impact crater, and the K-T boundary in the Alabama Gulf Coastal Plain; Wetumpka, Alabama; Wetumpka Field Forum 2007 Guidebook and Abstracts. Eds. King, D.T., Jr. and Ormö, J. 94−95.

DISSERTATIONES GEOLOGICAE UNIVERSITATIS TARTUENSIS

1. **Пээп Мянник.** Конодонты в верхнеордовикских и нижнесилурийских отложениях Эстонии. Тарту, 1992, 355 с.
2. **Elvi Tavast.** Fennoskandia kilbi lõunanõlva ja sellega piirnevate alade aluspõhja reljeef. Tartu, 1992, 357 lk.
3. **Kaarel Orviku.** Characterisation and evolution of Estonian seashores. Tartu, 1992, 19 p.
4. **Анатолий Молодьков.** ЭПР-анализ скелетного вещества моллюсков в хроностратиграфических исследованиях позднего кайнозоя. Тарту, 1992, 33 с.
5. **Jaan Lutt.** Late- and postglacial deposits on the Estonian shelf. Tartu, 1993, 31 p.
6. **Reet Karukäpp.** Gotiglatsiaalne morfogenees Skandinaavia mandriliustiku kagusektoris. Tartu, 1997, 181 p.
7. **Argo Jõeleht.** Geothermal studies of the Precambrian basement and Phanerozoic sedimentary cover in Estonia and Finland. Tartu, 1998, 125 p.
8. **Jüri Nemliher.** Mineralogy of Phanerozoic skeletal and sedimentary apatites: an XRD study. Tartu, 1999, 134 p.
9. **Kalle Kirsimäe.** Clay mineral diagenesis on the Lower Cambrian "Blue Clay" in the northern part of the Baltic Paleobasin. Tartu, 1999, 113 p.
10. **Jüri Plado.** Gravity and magnetic signatures of meteorite impact structures. Tartu, 2000, 87 p.
11. **Olev Vinn.** Morphogenesis and phylogenetic relationships of Clitambonitidines, Ordovician Brachiopods. Tartu, 2001, 127 p.
12. **Leho Ainsaar.** The middle Caradoc facies and faunal turnover in the late Ordovician Baltoscandian palaeobasin: sedimentological and carbon isotope aspects. Tartu, 2001, 109 p.
13. **Oive Tinn.** Early Ostracode evolution and Palaeoenvironmental application in the Ordovician of Baltoscandia. Tartu, 2002, 145 p.
14. **Maris Rattas.** Subglacial environments in the formation of drumlins — The case of the Saadjärve Drumlin Field, Estonia. Tartu, 2004, 117 p.
15. **Ene Kadastik.** Upper-Pleistocene stratigraphy and deglaciation history in northwestern Estonia. Tartu, 2004, 129 p.
16. **Helje Pärnaste.** Early Ordovician trilobites of suborder Cheirurina in Estonia and NW Russia: systematics, evolution and distribution. Tartu, 2004, 138 p.
17. **Mari-Ann Mõtus.** Silurian (Llandovery-Wenlock) tabulate corals of Baltoscandia: taxonomy, palaeoecology, distribution. Tartu, 2005, 167 p.
18. **Alar Rosentau**. Development of proglacial lakes in Estonia. Tartu, 2006, 114 p.
19. **Evelin Verš.** Development of impact-induced hydrothermal system at Kärdla impact structure. Tartu, 2006, 96 p.

20. **Sigitas Radzevičius.** The genus *Pristiograptus* in wenlock of East Baltic and the Holy Cross Mountains. Tartu, 2007, 133 p.
21. **Andres Marandi.** Natural chemical composition of groundwater as a basis for groundwater management in the Cambrian-Vendian aquifer system in Estonia. Tartu, 2007, 116 p.
22. **Eve Niinemets.** Vegetation and land-use history of the Haanja Heights (SE-Estonia) during the holocene. Tartu, 2008, 146 p.
23. **Kalle-Mart Suuroja.** Geology and lithology of the early palaeozoic marine impact stuctures Kärdla and Neugrund (Estonia). Tartu, 2008, 234 p.
24. **Rutt Hints.** Early diagenesis of Ordovician and Silurian Bentonites in the Northern Baltic Palaeobasin. Tartu, 2009, 90 p.
25. **Peeter Somelar.** Illitization of K-bentonites in the Baltic Basin. Tartu, 2009, 118 p.
26. **Ulla Preeden.** Remagnetizations in sedimentary rocks of Estonia and shear and fault zone rocks of southern Finland. Tartu, 2009, 121 p.
27. **Kati Tänavsuu-Milkeviciene.** Transgressive to regressive turnaround in the Middle Devonian Baltic Basin. Tartu, 2009, 106 p.
28. **Valle Raidla.** Chemical and isotope evolution of groundwater in the Cambrian-Vendian aquifer system in Estonia. Tartu, 2010, 134 p.
29. **Kadri Sohar.** Quaternary ostracods from Estonia and their application in palaeoenvironmental reconstruction. Tartu, 2010, 140 p.
30. **Kristjan Urtson.** Stepwise melt transport and accumulation: analogue and numerical modelling approach. Tartu, 2011, 83 p.
31. **Marko Kohv.** Landslides in clayey soils of western Estonia. Tartu, 2011, 116 p.
32. **Nele Muttik.** Post-impact alteration of impactites: Ries crater, Germany. Tartu, 2011, 78 p.
33. **Annette Sedman.** Strength and self-cementing properties of oil shale retorting wastes. Tartu, 2013, 82 p.
34. **Arkady Tsyrulnikov.** Complex seismo-acoustic and lithological study of the Lateglacial and postglacial sediments northern Gulf of Riga, eastern branch of the central Baltic Sea. Tartu, 2013, 102 p.
35. **Marge Uppin.** Geological sources and hydrochemistry of fluoride and boron in Silurian-Ordovician aquifer system. Tartu, 2013, 86 p.
36. **Peeter Talviste**. Temporal changes in weak natural and artificial soils – influence on geotechnical characteristics. Tartu, 2014, 204 p.
37. **Katrin Lasberg.** Chronology of the Weichselian Glaciation in the south-eastern sector of the Scandinavian Ice Sheet. Tartu, 2014, 100 p.
38. **Sirle Liivamägi**. Neoproterozoic Baltic paleosol: geology and paleoenvironmental interpretation. Tartu, 2015, 94 p.
39. **Lauri Joosu**. Petrography and the rare earth element composition of apatite in 2 Ga Onega and Pechenga basins, Russia: the environmental settings for phosphogenesis. Tartu, 2015, 139 p.
40. **Liisa Lang.** Baculate shell structure in Early Palaeozoic linguliform brachiopods. Tartu, 2015, 114 p.
41. **Päärn Paiste**. Geopolymeric potential of the Estonian oil shale processing waste. Tartu, 2017, 125 p.